# Buoyancy of Convective Vertical Motions in the Inner Core of Intense Hurricanes. Part I: General Statistics

MATTHEW D. EASTIN AND WILLIAM M. GRAY

*Department of Atmospheric Science, Colorado State University, Fort Collins, Colorado*

PETER G. BLACK

*Hurricane Research Division, NOAA/AOML, Miami, Florida*

(Manuscript received 19 December 2003, in final form 19 July 2004)

ABSTRACT

The buoyancy of hurricane convective vertical motions is studied using aircraft data from 175 radial legs collected in 14 intense hurricanes at four altitudes ranging from 1.5 to 5.5 km. The data of each leg are initially filtered to separate convective-scale features from background mesoscale structure. Convective vertical motion events, called cores, are identified using the criteria that the convective-scale vertical velocity must exceed 1.0 m $s^{-1}$ for at least 0.5 km. A total of 620 updraft cores and 570 downdraft cores are included in the dataset. Total buoyancy is calculated from convective-scale virtual potential temperature, pressure, and liquid water content using the mesoscale structure as the reference state.

Core properties are summarized for the eyewall and rainband regions at each altitude. Characteristics of core average convective vertical velocity, maximum convective vertical velocity, and diameter are consistent with previous studies of hurricane convection. Most cores are superimposed upon relatively weak mesoscale ascent. The mean eyewall (rainband) updraft core exhibits small, but statistically significant, positive total buoyancy below 4 km (between 2 and 5 km) and a modest increase in vertical velocity with altitude. The mean downdraft core not superimposed upon stronger mesoscale ascent also exhibits positive total buoyancy and a slight decrease in downward vertical velocity with decreasing altitude. Buoyant updraft cores cover less than 5% of the total area in each region but accomplish ~40% of the total upward transport.

A one-dimensional updraft model is used to elucidate the relative roles played by buoyancy, vertical perturbation pressure gradient forces, water loading, and entrainment in the vertical acceleration of ordinary updraft cores. Small positive total buoyancy values are found to be more than adequate to explain the vertical accelerations observed in updraft core strength, which implies that ordinary vertical perturbation pressure gradient forces are directed downward, opposing the positive buoyancy forces. Entrainment and water loading are also found to limit updraft magnitudes.

The observations support some aspects of both the hot tower hypothesis and symmetric moist neutral ascent, but neither concept appears dominant. Buoyant convective updrafts, however, are integral components of the hurricane's transverse circulation.

## 1. Introduction

Great strides in understanding hurricane internal structure, dynamics, and evolution have been made since instrumented aircraft began routine penetrations. However, our understanding of inner-core cumulus convection remains limited, despite its well-recognized crucial role. Two fundamental properties used to describe the nature of cumulus convection are vertical velocity and buoyancy. Several studies have utilized aircraft observations to document the vertical velocity characteristics of hurricanes (Gray 1965; Jorgensen et al. 1985; Black et al. 1994; Black et al. 1996). Observational estimates of buoyancy, however, have been limited by the inability to collect accurate thermodynamic observations within convection due to the wetting of aircraft sensors (e.g., Eastin et al. 2002a,b).

Despite inadequate thermodynamic observations, previous studies of hurricane inner-core (defined here as within 150 km of storm center) convection have provided circumstantial evidence suggesting the presence of significant local buoyancy. Jorgensen et al. (1985, hereafter JZL) analyzed vertical motions at altitudes between 0.5 and 6.1 km in the eyewalls and rainbands of four intense hurricanes. Their strongest 10% of updrafts (>4 m $s^{-1}$) exhibited a modest increase in strength (~2–4 m $s^{-1}$) with altitude, implying a vertical

*Corresponding author address:* Matthew D. Eastin, Department of Math and Computer Science, Central College, 812 University, Pella, IA 50219.
E-mail: eastinm@central.edu

acceleration. Subsequent statistical summaries of hurricane vertical motions were consistent with JZL (Black et al. 1994; Black et al. 1996). JZL also discussed observations from a unique traverse along Hurricane Allen's (1980) eyewall; multiple relative updraft maxima $>10$ m s$^{-1}$ over scales $< 5$ km were embedded within a sustained (organized) updraft in which upward vertical velocities $>3$ m s$^{-1}$ were continuously observed over ~40 km. Marks and Houze (1987) observed similar discrete updraft maxima superimposed upon sustained motions in Hurricane Alicia's (1983) eyewall. Finally, the extreme vertical velocities ($>10$ m s$^{-1}$) found in hurricane "supercells" (Gentry et al. 1970; Black et al. 1986; Ebert and Holland 1992; Black et al. 1994; Heymsfield et al. 2001) are also indicative of appreciable local buoyancy.

Several studies have provided estimates of convective available potential energy (CAPE), or the maximum potential buoyancy, in hurricanes from either individual sounding databases (Sheets 1969; Frank 1977; Bogner et al. 2000) or composited flight-level data at multiple altitudes (Gray and Shea 1973; Jorgensen 1984b). Consensus suggests that inner-core CAPE is small ($<1200$ J kg$^{-1}$) and decreases toward neutral stability upon approach to the eyewall. Note, however, that only minimal positive CAPE ($<200$ J kg$^{-1}$) would be required to explain the strongest vertical velocities observed in hurricanes (~20 m s$^{-1}$).

Theoretical and numerical studies have also provided insight into the organization of hurricane vertical motions and the role of buoyancy in storm evolution. Malkus and Riehl (1960) speculated that a large fraction of the required vertical mass transport was accomplished rapidly by a few undilute buoyant updrafts, or "hot towers," rather than by a more uniform ring of gradual ascent. In contrast, Emanuel (1986) argued that the hurricane inner core is often close to a state of moist slantwise neutrality, such that symmetric hurricane-like vortices can evolve with negligible contributions from buoyant updrafts. Two recent analyses of three-dimensional nonhydrostatic hurricane simulations have furthered the debate. Zhang et al. (2000) analyzed the vertical momentum budget of the temporally and azimuthally averaged eyewall, and attributed small accelerations in the mean vertical velocity to upward-directed perturbation pressure gradient forces. In contrast, Braun (2002) analyzed the vertical momentum budget along individual updraft trajectories in the eyewall and attributed updraft accelerations to positive local buoyancy forces. The contrast between theories and between simulation results raises the question of whether asymmetric buoyant convection is an integral component of inner-core structure and evolution.

Clearly, information concerning buoyancy is needed to provide a more thorough description of how hurricane convection behaves and interacts with the vortex. Accurate observational estimates of buoyancy require reliable thermodynamic data within convection. In recent years short-path radiometric thermometers have been installed on research aircraft. Lawson and Cooper (1990) demonstrated that such radiometers can provide accurate flight-level air temperatures in and near convection without the adverse effects of sensor wetting. Several studies of ordinary tropical oceanic convection (Jorgensen and LeMone 1989; Lucas et al. 1994; Wei et al. 1998; Igau et al. 1999) have effectively used radiometric temperatures to analyze buoyancy within convective updrafts and downdrafts.

The objective of this study is to build upon previous research of hurricane convection by providing a statistical summary of the local buoyancy force acting on meaningful convective-scale vertical motions within the inner-core of intense hurricanes. We employ a large radial leg database with the more reliable radiometric temperatures. This paper, which is Part I of a two-paper series, describes the data and methodology used to identify and examine convective-scale vertical motions, presents summary statistics of their kinematic and buoyancy characteristics as a function of altitude and region (eyewall and rainband), documents the fractional contribution of buoyant updrafts to the total upward mass transport, and elucidates the relative role played by buoyancy in vertically accelerating ordinary convective updrafts. In Part II (Eastin et al. 2005), case studies of two hurricanes are used to illustrate the typical azimuthal distribution of buoyant convection, demonstrate that the low-level eye can be an important source region of buoyant eyewall convection, and provide evidence of three physical links between buoyant convection and storm evolution.

## 2. Data and methodology

### *a. Description of data used*

The data used in this study were collected by the two National Oceanic and Atmospheric Administration (NOAA) WP-3D aircraft during 25 flights into 11 Atlantic and 3 eastern Pacific intense hurricanes from 1988 to 1998 (see Table 1). The basic flight-level instrumentation and radar systems on the aircraft are described in Jorgensen (1984a); more detailed descriptions of the thermodynamic sensors are given in Eastin et al. (2002a). The flight-level data were recorded at a 1-Hz rate during each flight and then postprocessed at the NOAA Hurricane Research Division (HRD) into radial legs using methods described in Willoughby et al. (1982), Willoughby and Chelmow (1982), and Samsury and Zipser (1995). Each radial leg extends up to 150 km from the storm center and consists of storm-relative observations of the three-dimensional wind field in cylindrical coordinates, temperature, dewpoint, cloud water content, geopotential height, and the aircraft position. Data within each radial leg are distributed into 0.5-km average bins by an overlapping triangular-shaped filter with a 2-km window. A total of 175 radial

TABLE 1. Summary of flight-level data used in this study.

| Storm | Date yr/mo/day | Storm intensity (mb) | Flight ID | Flight Altitude (km) | No. of legs | Mean leg length (km) | Vertical velocity extremes* Max $w$ (m s$^{-1}$) | Vertical velocity extremes* Min $w$ (m s$^{-1}$) | No. of cores** Up | No. of cores** Down |
|---|---|---|---|---|---|---|---|---|---|---|
| Gilbert | 88/09/11 | 969 | I | 3.0 | 8 | 90 | 9.8 | −6.5 | 32 | 22 |
| | 88/09/14 | 891 | H | 3.0 | 10 | 116 | 9.4 | −5.0 | 33 | 35 |
| | 88/09/15 | 950 | I1 | 1.5 | 8 | 132 | 2.1 | −1.4 | 10 | 4 |
| | | 947 | I2 | 1.5 | 8 | 127 | 3.4 | −2.3 | 13 | 9 |
| Joan | 88/10/21 | 950 | I | 1.5 | 6 | 102 | 6.0 | −1.6 | 17 | 11 |
| Gabrielle | 89/09/03 | 932 | H | 3.0 | 2 | 66 | 2.8 | −1.4 | 3 | 4 |
| Hugo | 89/09/15 | 919 | I | 5.5 | 4 | 95 | 5.7 | −3.3 | 6 | 7 |
| | 89/09/18 | 958 | I | 4.2 | 4 | 93 | 4.8 | −3.7 | 15 | 13 |
| | 89/09/21 | 941 | I | 4.2 | 6 | 102 | 6.0 | −3.6 | 26 | 24 |
| Gustav | 90/08/30 | 960 | I | 1.5 | 6 | 61 | 5.3 | −3.5 | 17 | 13 |
| Jimena | 91/09/23 | 948 | I | 1.5 | 2 | 87 | 9.9 | −11.2 | 4 | 5 |
| | | | | 3.0 | 10 | 68 | 10.0 | −12.1 | 33 | 31 |
| | | | H | 3.0 | 3 | 65 | 11.8 | −4.9 | 14 | 7 |
| | | | | 4.2 | 1 | 59 | 6.9 | −1.5 | 3 | 3 |
| | 91/09/24 | 950 | I | 3.0 | 4 | 93 | 6.5 | −2.4 | 14 | 12 |
| Emily | 93/08/31 | 964 | I | 5.5 | 4 | 120 | 4.6 | −3.1 | 15 | 14 |
| Olivia | 94/09/24 | 952 | I | 4.2 | 5 | 71 | 16.0 | −3.1 | 16 | 12 |
| | 94/09/25 | 930 | I | 4.2 | 11 | 75 | 6.6 | −3.9 | 31 | 29 |
| Luis | 95/09/04 | 940 | I | 5.5 | 11 | 100 | 8.5 | −5.0 | 40 | 34 |
| | 95/09/07 | 937 | I | 4.2 | 4 | 124 | 6.6 | −2.2 | 13 | 17 |
| Opal | 95/10/04 | 937 | I | 4.2 | 4 | 126 | 5.5 | −2.7 | 19 | 14 |
| Edouard | 96/08/26 | 939 | I | 3.0 | 8 | 117 | 8.2 | −5.6 | 39 | 47 |
| | 96/08/27 | 941 | I | 3.0 | 14 | 103 | 9.8 | −5.8 | 64 | 59 |
| Fran | 96/09/05 | 952 | I | 1.5 | 4 | 113 | 1.7 | −1.7 | 6 | 10 |
| Guillermo | 97/08/02 | 950 | I | 5.5 | 12 | 105 | 12.3 | −4.6 | 49 | 50 |
| | 97/08/03 | 923 | I | 5.5 | 12 | 91 | 14.3 | −5.6 | 71 | 64 |
| Georges | 98/09/19 | 939 | H | 4.2 | 4 | 75 | 12.6 | −4.8 | 17 | 20 |
| Total | | | | | 175 | | | | 620 | 570 |

* Determined from 0.5-km total vertical velocity ($w$) data prior to filtering.
** Defined from convective-scale vertical velocity ($w_c$) data after filtering. See text for definition.

legs at reference pressure levels of 850, 700, 600, and 500 mb were used. In addition, radar reflectivity from the tail X-band radar was used to estimate flight-level precipitation water content.

### *b. Data treatment*

The vertical velocity ($w$) along each radial leg was computed using techniques similar to those described in JZL. These methods yield an absolute accuracy of $\pm 1$ m s$^{-1}$ for $w$ during straight and level flight. JZL noted that the zero vertical velocity was typically offset 0.1–0.4 m s$^{-1}$ in nonconvective regions outside the eyewall and between rainbands because of a known drift in the vertical accelerometer, and such offsets could lead to the anomalous identification of updrafts and downdrafts. Assuming the actual vertical velocity in nonconvective regions is close to zero, leg average offsets were determined from the $|w| < 1.5$ m s$^{-1}$ data and removed. The 1.5 m s$^{-1}$ threshold was used to isolate nonconvective regions with consideration for the absolute accuracy of the computed vertical velocities. Offsets were typically less than 0.3 m s$^{-1}$.

The temperatures and dewpoints included in the HRD radial leg database were measured by Rosemount and General Eastern instruments, respectively, which are susceptible to errors induced by sensor wetting in clouds and precipitation (LeMone 1980; Lawson and Cooper 1990; Eastin et al. 2002a). During wetting, the temperature sensor behaves more like a wet-bulb thermometer and reports erroneously low values, while the chilled-mirror dewpoint probe measures erroneously high values. To effectively circumvent these errors, temperatures from a more accurate short-path radiometer were used in combination with the General Eastern dewpoints following the procedures outlined by Eastin et al. (2002a). The resulting temperatures and dewpoints were extrapolated along moist adiabats from their reference pressure levels of 850, 700, 600, and 500 mb to reference altitudes of 1.5, 3.0, 4.2, and 5.5 km, respectively. Pressure ($p$) was then recomputed for each radial leg at the reference altitude. This extrapolation was applied for consistency with our buoyancy definition (see section 2c) and does not affect the results. Finally, virtual potential temperature ($\theta_v$) was computed along each radial leg from the thermodynamic data.

Cloud water content ($q_c$) was measured by a Johnson–Williams "hot wire" probe designed to be sensitive to drops <0.06 mm in diameter. However, several stud-

ies (Spyers-Duran 1968; Merceret and Schricker 1975; Feind et al. 2000) have found the probe to undersample cloud drops >0.03 mm in diameter and not respond well to $q_c$ <0.05 g m$^{-3}$. As a result, $q_c$ may be underestimated by a factor as large as 3, depending primarily upon drop concentrations at the large end of the cloud droplet spectrum. Eastin (2003) demonstrated that any such underestimations have a negligible effect on the results due to the definition of buoyancy and reference state used. Baumgardner (1983) also noted the probe can suffer from out-of-cloud baseline drifting, and only upon drift removal is the absolute accuracy (±20%) attainable. Any apparent baseline drifting was manually removed after visual inspection of $q_c$ profiles.

Precipitation water content ($q_r$) was estimated from tail radar reflectivity values adjacent to the aircraft at flight level. The tail radar completes one rotation every 6 s in the vertical plane normal to the aircraft track. As a result, the radar antenna measures reflectivity along a horizontally incident path (i.e., at flight level) every 3 s. The range gate length (75, 150, or 300 m) and range delay (0–400 m) vary from flight to flight. Therefore, a mean flight-level reflectivity ($Z$) was determined from reflectivity values in the ~750 m equivalent range gate of the two horizontally incident pulse volumes. At typical ground speeds of ~125 m s$^{-1}$, values of $Z$ were obtained on each side of the aircraft at ~0.75 km intervals. The $Z$ values were thus linearly interpolated to the 0.5-km resolution of the radial legs. Finally, the $Z$ were converted to $q_r$ using the empirical relationships

$$Z = \begin{Bmatrix} 14630\, q_r^{1.4482} & \text{for rain} \\ 670\, q_r^{1.79} & \text{for ice} \end{Bmatrix}, \tag{1}$$

where $Z$ is expressed in units of mm$^6$ m$^{-3}$, and $q_r$ is in units of g m$^{-3}$. The bulk relationships for rain and ice were obtained from Gamache et al. (1993) and Black (1990), respectively, and were derived from Particle Measuring System (PMS) probe data collected in hurricanes.[1] Since strong updrafts (>5 m s$^{-1}$) can carry liquid water several kilometers above the freezing level (Black and Hallett 1986), $q_r$ is computed as a linear combination of the rain and ice relationships at flight-level temperatures between 0° and −20°C. This procedure may underestimate the *absolute* values of $q_r$ in weak convection above the freezing level, but *relative radial differences* (used here) are unaffected.[2] Furthermore, this procedure allows for the observed radial variation in freezing level while eliminating step functions in $q_r$ across 0°C that are not observed (JZL; Black et al. 1996; Cecil et al. 2002).

[1] The reflectivity-based $q_r$ were used since PMS data were only available for a few flights.

[2] Use of warmer thresholds for complete glaciation (−10° and −5°C) resulted in maximum water loading and total buoyancy differences of only 0.015 K.

### c. Definitions of buoyancy and reference state

The definitions of buoyancy and its reference state are not unique. The key is to effectively separate the appropriate balanced state from any locally unbalanced disturbances. The conventional wisdom for isolated convection implies that hydrostatic balance dominates and the reference state can be well represented by the horizontally homogeneous clear air within a few hundred kilometers of the convection. Hurricane convection, however, is superimposed upon a slowly evolving transverse circulation and a quasi-symmetric vortex near both hydrostatic and gradient wind balance. As a result, the appropriate balanced state for hurricane convection is not readily apparent. Zhang et al. (2000) defined the reference state locally through a running average of four adjacent model grid points. Braun (2002) defined the reference state as the low-wavenumber (0 and 1) storm structure.

Here, we define a *local* reference state through application of a running Bartlett filter (Jenkins and Watts 1968) with a 20-km window to the $\theta_v$, $p$, $q_c$, $q_r$, and $w$ data of each radial leg. The motivation for this definition and its application is as follows. First, Willoughby (1979, 1990) found through data and scale analysis that hydrostatic and gradient wind balance were good approximations for the slowly evolving symmetric vortex on radial scales greater than 15 km (i.e., mesoscales). Montgomery and Franklin (1998) have also shown that low-wavenumber (e.g., 1–4) structures of the hurricane inner core satisfy the criteria for asymmetric balance (Shapiro and Montgomery 1993). Inspection of radar reflectivity fields for each hurricane (e.g., Fig. 1) reveals that slowly evolving symmetric and low-wavenumber features with radial scales of ~15 km are prevalent, and in some cases the features propagate azimuthally. Thus, application of the filter to each radial leg of any given flight pattern (e.g., Fig. 1) will act to capture the balanced symmetric and low-wavenumber fields without concern for the orientation of such features with respect to the flight pattern. Second, Shapiro and Willoughby (1982) demonstrated that persistent realistic sources (or sinks) of heat and momentum introduced to a balanced vortex will induce a slowly evolving secondary circulation on mesoscales. We thus applied the filter to the $w$ of each radial leg in order to capture the balanced mesoscale vertical motion. Third, Zhang et al. (2000) and Braun (2002) found that the symmetric and low-wavenumber components of liquid water content contribute to hydrostatic balance, and thus the filter was also applied to the $q_c$ and $q_r$ fields of each radial leg. Clearly, our reference state definition was designed to effectively separate the slowly evolving (i.e., balanced) mesoscale structure from any transient convective-scale features in a manner consistent with both theory and observations.

We follow Braun (2002) and define total buoyancy ($B$) as

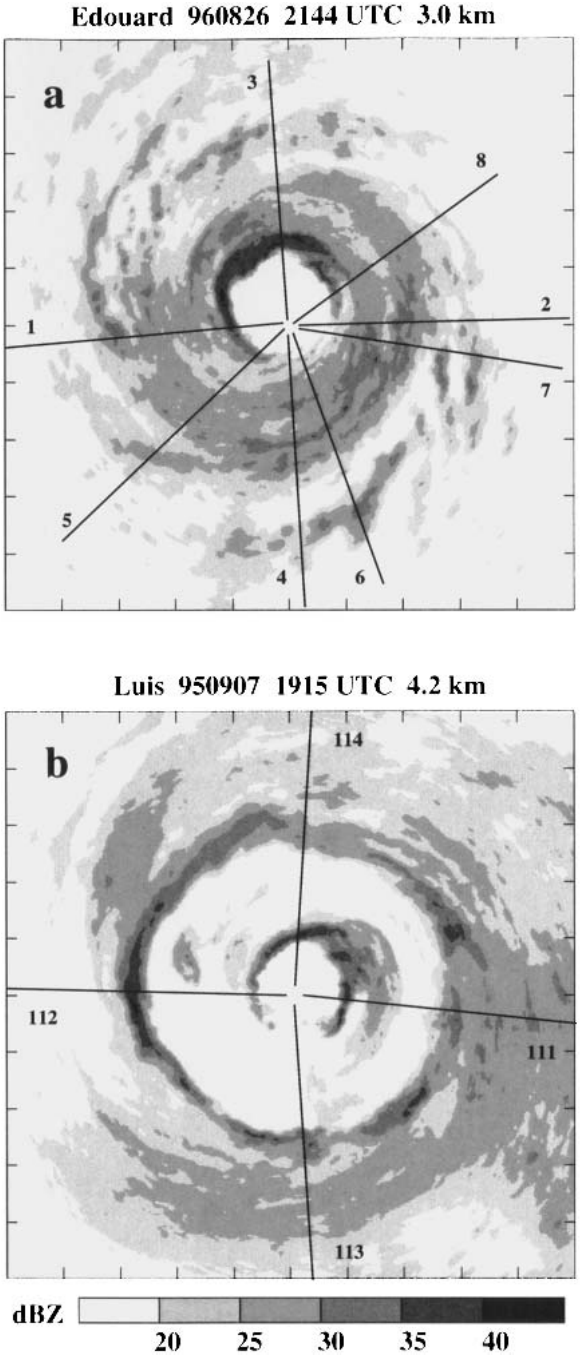


FIG. 1. Lower-fuselage horizontal radar reflectivity in (a) Hurricane Edouard at 2144 UTC on 26 Aug 1996 at ~3.0-km altitude, and (b) Hurricane Luis at 1915 UTC on 7 Sep 1995 at ~4.2-km altitude. Note that both eyewalls are dominated by a gross wavenumber-1 reflectivity field and that the rainband (or outer eyewall) reflectivity in Luis is more symmetric. Bold lines denote the radial legs flown, and leg numbers denote the order in which the legs were flown. Note the even azimuthal distribution of the radial legs. The domain of each panel is 240 km × 240 km, tick marks are shown every 24 km, and the reflectivity scale is shown at the bottom.

$$B = \underbrace{\left[ g \frac{\theta_v'}{\overline{\theta}} \right]}_{\text{TB}} + \underbrace{\left[ g(\kappa - 1) \frac{p'}{\overline{p}} \right]}_{\text{DB}} + \underbrace{[-g(q_c' + q_r')]}_{\text{WL}}, \quad (2)$$

where $\kappa = 0.286$, $g$ is the gravitational acceleration, overbars represent the mesoscale reference state, and primes denote convective-scale perturbations from the reference state. The three contributions to $B$ are referred to here as thermal buoyancy (TB), dynamic buoyancy (DB), and water loading (WL). As noted by Braun (2002), the definition of total buoyancy is independent of whether air motions are purely vertical or along slantwise paths; nonzero total buoyancy will induce local accelerations in the vertical component.

Shown on the lhs of Fig. 2 are the total and reference state $w$, $\theta_v$, $p$, $q_c$, and $q_r$ fields for a representative radial leg flown from 2144–2158 UTC 26 August 1996 in Hurricane Edouard at 3-km altitude (leg 8 in Fig. 1a). The filtered profiles effectively capture the mesoscale warm-core structure and are comparable to results from observational (Shea and Gray 1973; Barnes et al. 1983; Jorgensen 1984a,b; Marks et al. 1992) and numerical (Rotunno and Emanuel 1987; Liu et al. 1999; Wang 2002) studies of mesoscale inner-core structure. Shown on the rhs of Fig. 2 are the perturbation (or convective) vertical velocity ($w_c$) and each buoyancy term in Eq. (2) calculated from the lhs profiles. A comparison of $w_c$ with TB (or $B$) reveals that each appreciable convective-scale updraft event (denoted by a vertical line) is locally buoyant along this radial leg. Also, note that TB dominates $B$ with only small contributions from DB and WL.

Since the focus of this study is to determine characteristics of meaningful convective-scale vertical velocity events, and these events are defined *after* the reference state (see section 2d), our results may be sensitive to the reference state definition. The use of a 20-km filter window was somewhat arbitrary but consistent with theory and observations. Use of smaller filter windows (10–18 km) decreased the number of events since a larger fraction of total vertical velocity was included in the reference state. In contrast, larger filter windows (22–30 km) increased the number of events, but also prevented adequate sampling of the eyewall during some flights since events could not be defined in the first half-window of each leg. Despite differences in numbers, application of a standard two-tailed Student's $t$ test revealed no significant differences in distribution means (at the 95% level) for any event magnitude or buoyancy parameter. Therefore, our results are effectively independent of the filter window size used to represent the reference state.

Given that our methodology to determine the reference state is also a scale separation, we hereafter (for simplicity) refer to the reference state as the "mesoscale" structure and perturbations from the reference state as the "convective" structure.

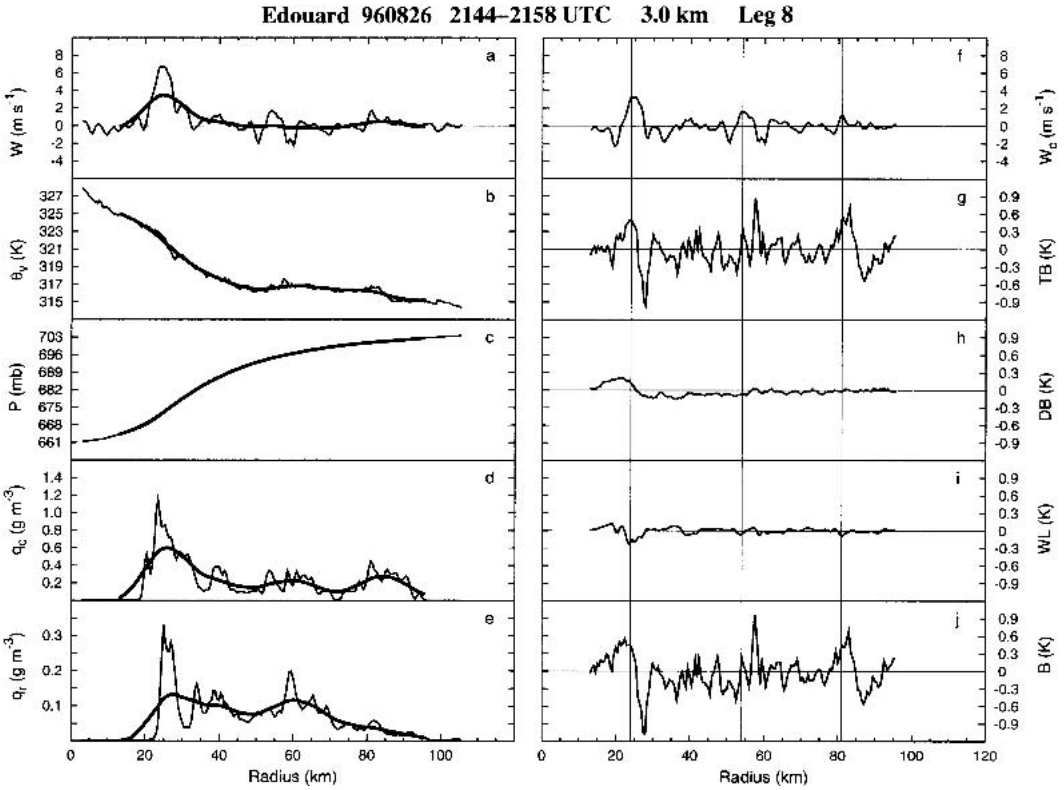


FIG. 2. Storm-relative radial profiles of (a) total vertical velocity $w$, (b) virtual potential temperature $\theta_v$, (c) pressure $P$, (d) cloud water content $q_c$, (e) precipitation water content $q_r$, (f) convective vertical velocity $w_c$, (g) thermal buoyancy TB, (h) dynamic buoyancy DB, (i) water loading WL, and (j) total buoyancy $B$ for radial leg 8 in Hurricane Edouard at ~3.0 km on 26 Aug 1996 from 2144 to 2158 UTC. Bold lines in (a)–(e) are the mesoscale profiles, or reference state, determined from application of a 20-km running Bartlett filter to the data. Vertical lines in (f)–(j) denote identified convective updraft cores. Note that each updraft core is positively buoyant. Further note that values of TB, DB, WL, and $B$ are depicted on the same scale, and that TB is the dominant term in $B$. See text for definitions of $w_c$, TB, DB, WL, and $B$.

### *d. Definition of convective vertical velocity cores*

JZL used 1-Hz flight-level data with ~125 m resolution to define meaningful vertical velocity events, called cores, for which $|w|$ exceeds 1 m s$^{-1}$ over a minimum horizontal extent of 0.5 km. Note that JZL defined their cores from the *total* vertical velocity. Here, we wish to remove any slowly evolving mesoscale vertical velocity signature prior to core identification in order to isolate the more transient convective-scale motions. Therefore, updraft and downdraft cores are defined from the *convective* vertical velocity when $|w_c|$ exceeds 1 m s$^{-1}$ for at least 0.5 km. These definitions are thus analogous to those used by JZL and are designed to separate meaningful convective events from turbulent features. The vertical lines in Fig. 2 denote identified updraft cores.

A total of 620 updraft cores and 570 downdraft cores are included in the database. Several characteristics of each core are summarized: the maximum 0.5-km convective vertical velocity ($w_{c\ \max}$) within the core; average convective vertical velocity ($\overline{w}_c$); average mesoscale vertical velocity ($\overline{w}_m$); diameter (DIAM, or distance along the radial leg); average thermal buoyancy ($\overline{\text{TB}}$); average dynamic buoyancy ($\overline{\text{DB}}$); average water loading ($\overline{\text{WL}}$); and average total buoyancy ($\overline{B}$). For each core we also computed average relative humidity ($\overline{\text{RH}}$), average total vertical velocity ($\overline{w}$), average total liquid water content ($\overline{q}_l$, the sum of $q_c$ and $q_r$), and average equivalent potential temperature ($\overline{\theta}_e$) following Bolton (1980).

### *e. Determination of eyewall and rainband regions*

In order to separately determine buoyancy characteristics within eyewall and rainband convection, each radial leg was divided into two parts. Following procedures described by JZL, a cutoff radius was subjectively determined using lower-fuselage radar imagery and flight-level data to include all eyewall convection inward of this cutoff. The rainband region, which also includes stratiform precipitation and relatively rain-free areas, is located outside the cutoff radius. In general, the cutoff radius was ~15 km outside the radius of maximum wind (RMW). The eyewall was typically identified as the innermost quasi-annular ring of convection. In a few cases, the innermost convection in-

cluded in the eyewall region was an asymmetric band near the RMW that spiraled inward. If the innermost convection was composed of numerous convective bands within 15 km of one another, all the bands were included in the eyewall region. Concentric outer eyewalls (Willoughby et al. 1982) were included in the rainband region if they were >15 km from a distinct inner eyewall (e.g., Fig. 1b) and exhibited relatively weak thermodynamic radial gradients. These procedures account for the variability of the eyewall radius as well as asymmetries from storm to storm.

### f. Data representativeness

The hurricanes included in this study were required to either possess maximum sustained winds in excess of 50 m $s^{-1}$ or a minimum surface pressure below 965 mb during the flight. No further criteria were used. The different character of each hurricane undoubtedly contributes to variability in the statistics. During each flight, the aircraft typically flew figure-four patterns with headings at approximately right angles to the wind direction. Thus, the radial legs within a given storm were evenly distributed about the storm center, and convection was frequently sampled despite any asymmetric storm structure. Radial leg lengths were ~100 km or more, and the eyewall region was always well sampled. Specific experiment goals during a few flights limited leg lengths and thus sampling of the rainband region. Moreover, most flights encountered relatively strong convection with maximum $w$ in excess of 5 m $s^{-1}$ (see Table 1). By combining numerous radial legs from multiple storms, we believe the dataset is representative of convection in the lower and middle troposphere of intense hurricanes and thus is adequate for performing a statistical analysis of inner-core convective vertical motions and their buoyancy.

Most cores were located within mesoscale features easily identified by radar as either an eyewall or rainband. A typical flight pattern prevents adequate temporal sampling of a given convective band by radar to determine the particular stage in the convective life cycle of an individual core. Thus, the data represent a random sample of growing, mature, and dissipating convection (as well as some strong mechanically generated turbulence and gravity waves). The large dataset and unique character of each storm should prevent a bias toward one particular stage.

A potential source of error could arise if the aircraft does not penetrate the core center. Assuming a circular core with maximum vertical velocity at the geometric center and a linear decay to the edge, JZL demonstrated that random penetrations of a given core would lead to an average underestimation of $w_{c\,\max}$ and $\overline{w}_c$ by a factor of 2, and DIAM would be underestimated by ~20%. Extending this reasoning to $\overline{\text{TB}}$, $\overline{\text{DB}}$, $\overline{\text{WL}}$, and $\overline{B}$ with the assumption that each maximizes at the geometric center, buoyancy parameters may also be underestimated by a factor of 2.

## 3. Results

### a. Cumulative distributions

Distributions of DIAM, $w_{c\,\max}$, $\overline{w}_c$, $\overline{w}_m$, $\overline{\text{TB}}$, $\overline{\text{DB}}$, $\overline{\text{WL}}$, and $\overline{B}$ were initially complied for updraft and downdraft cores of each region and altitude. All $w_{c\,\max}$, $\overline{w}_c$, and DIAM distributions were approximately lognormal. All $\overline{w}_m$, $\overline{\text{TB}}$, $\overline{\text{DB}}$, $\overline{\text{WL}}$, and $\overline{B}$ distributions were approximately normal, although $\overline{w}_m$ and $\overline{\text{DB}}$ tended to be poorer fits. As a result of the similarities, the distributions from each region and altitude were combined and are presented in Figs. 3 and 4 for convective updraft and downdraft cores within the hurricane inner core. Section 3b discusses altitude variations by region.

Cumulative distributions of convective core diameter and strength are shown in Figs. 3a–c in lognormal format. Updraft and downdraft DIAM distributions were nearly identical with a median size of ~1.5 km. Median $\overline{w}_c$ for updrafts and downdrafts were also similar, with magnitudes of 1.5 and −1.4 m $s^{-1}$, respectively, ~30% smaller than corresponding $\overline{w}_{c\,\max}$ values. The distributions clearly contain few large or strong events. Less than 5% of convective cores were >5 km in diameter or exceeded ±5 m $s^{-1}$ in average strength. The strongest $w_{c\,\max}$ encountered was 11.8 m $s^{-1}$ at 4.2-km altitude in the eyewall of Olivia. The strongest $w$ observed was 16.0 m $s^{-1}$, which is comparable to the maxima observed by JZL (17.2 m $s^{-1}$) and Black et al. (1994; 23.9 m $s^{-1}$) at similar altitudes in other intense hurricanes.

Also shown in Figs. 3a–c are the analogous JZL cumulative distributions of updraft and downdraft core diameter and strength estimated from *total* vertical velocity data within four intense hurricanes. The differences are largely attributable to the removal of $w_m$ from $w$ prior to convective core identification and differences in data resolution (Eastin 2003). Of interest here are the distribution shapes and gross magnitudes; the JZL distributions are approximately lognormal with diameters that rarely exceed 5 km and average strengths that rarely exceed ±5 m $s^{-1}$. The similarities provide strong evidence that the data used here and the data used by JZL are representative of similar populations. Such properties were also found by Black et al. (1996) using Doppler radar velocity data.

Cumulative distributions of convective core average mesoscale vertical velocity are shown in Fig. 3d in linear-normal format. Median $\overline{w}_m$ for updrafts and downdrafts were similar at ~0.5 m $s^{-1}$, or ~35% of the median $\overline{w}_c$ magnitudes. Most $\overline{w}_m$ range from −1 to 3 m $s^{-1}$, consistent with the aforementioned observational and numerical studies of mesoscale inner-core structure. Moreover, Fig. 3d demonstrates that some intense hurricane eyewalls are not quasi-symmetric rings of ascent, but rather have regions of organized mesoscale descent.

Cumulative distributions of convective core average buoyancy are shown in Fig. 4 in linear-normal format. Magnitudes of $\overline{\text{TB}}$, $\overline{\text{DB}}$, $\overline{\text{WL}}$, and $\overline{B}$ have been adjusted to

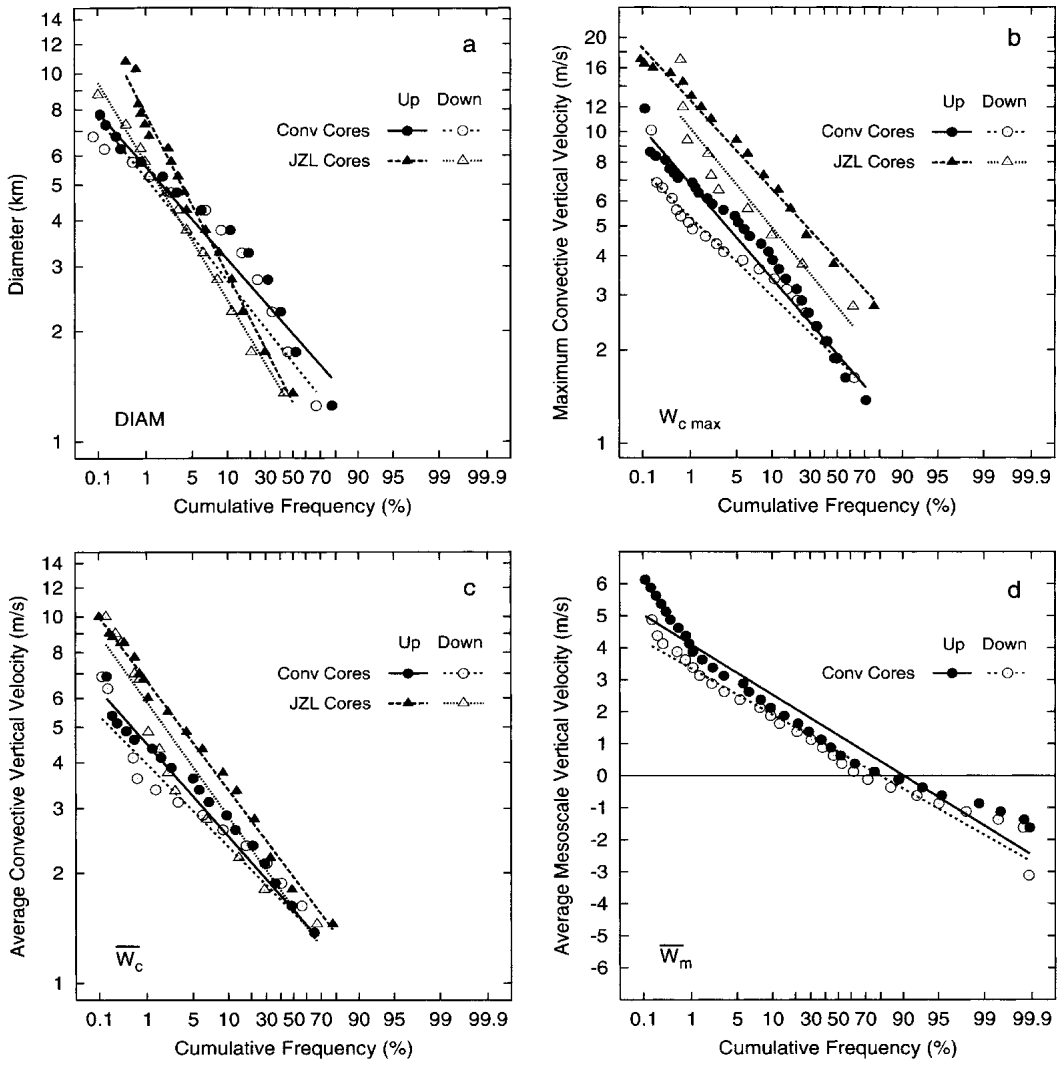


FIG. 3. Cumulative distributions of (a) diameter DIAM, (b) maximum convective vertical velocity $w_{c\,\max}$, (c) average convective vertical velocity $\overline{w}_c$, and (d) average mesoscale vertical velocity $\overline{w}_m$ for all convective updraft and downdraft cores. The analogous Jorgensen et al. (1985) core data from their Fig. 1 are also shown. The straight lines represent linear fits to the data.

the common unit of Kelvin for easier comparison with previous studies. Updraft *and* downdraft $\overline{B}$ range from 1.7 to −1.9 K with respective median values of 0.16 and −0.05 K. Corresponding median $\overline{\text{TB}}$ were 0.21 and −0.06 K. Clearly, the $\overline{B}$ values were dominated by the $\overline{\text{TB}}$ contribution; most $\overline{\text{DB}}$ and $\overline{\text{WL}}$ range over ±0.5 K and median values were less than ±0.05 K.

### *b. Stratification by eyewall and rainband region*

Differences between eyewall and rainband cores are elucidated by extracting summary statistics from the respective distributions at each altitude level (Figs. 5–7). Median and upper 10% (>90% of the sample) values were extracted from the DIAM, $w_{c\,\max}$ and $\overline{w}_c$ distributions. Means and standard deviations ($\sigma$) were extracted from the $\overline{w}_m$, $\overline{\text{TB}}$, $\overline{\text{DB}}$, $\overline{\text{WL}}$, and $\overline{B}$ distributions. Such statistics were selected to facilitate comparison with previous studies; alternative statistical measures (medians versus means) exhibit similar regional differences and vertical structure (Eastin 2003).

In both regions, updraft and downdraft core diameter and strength (Fig. 5) increased slightly with altitude. In the eyewall, median diameters increased ~1.0 km from 1.5- to 5.5-km altitude. Median updraft velocities increased 0.4 m s$^{-1}$ in $\overline{w}_c$ and 0.8 m s$^{-1}$ in $w_{c\,\max}$ before reaching a maximum at 4.2 km. For downdrafts, median $\overline{w}_c$ and $w_{c\,\max}$ increased 0.5 m s$^{-1}$ from 1.5 to 3.0 km; above that they changed little. The upper 10% statistics exhibit similar vertical structure but increase by more than twice their median counterparts over the same depths. Rainband cores were smaller and weaker

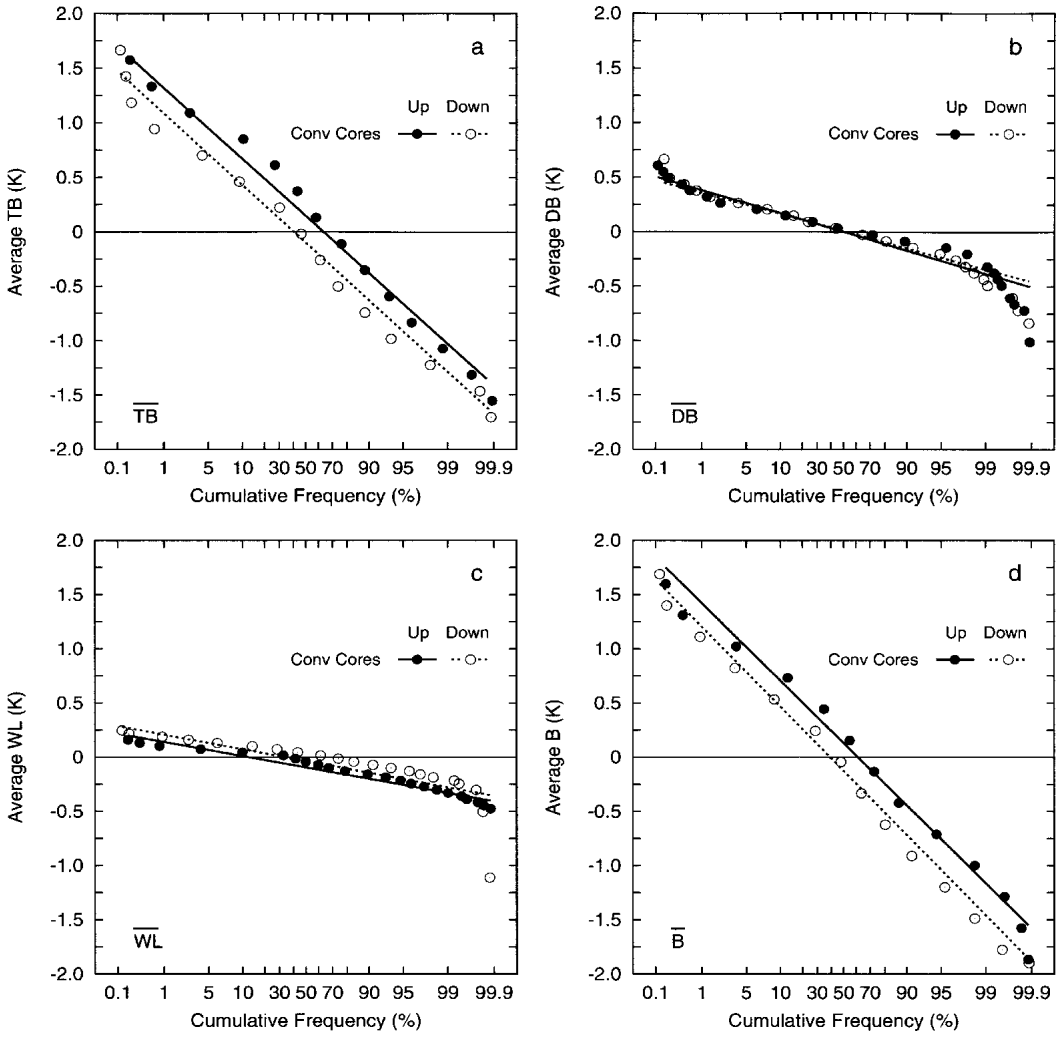


FIG. 4. Cumulative distributions of (a) average thermal buoyancy $\overline{\text{TB}}$, (b) average dynamic buoyancy $\overline{\text{DB}}$, (c) average water loading $\overline{\text{WL}}$, and (d) average total buoyancy $\overline{B}$ for all convective updraft and downdraft cores. The straight lines represent linear fits to the data.

than eyewall cores with less increase in each parameter with altitude. Overall, the statistics reflect a tendency for midlevel cores to be larger and stronger entities compared to low-level cores, consistent with the results of JZL and Black et al. (1996).

The mesoscale vertical motion (Fig. 6), upon which the convective cores are superimposed, also increased slightly with altitude in both regions. Mean $\overline{w}_m$ were positive at all altitudes, but rainband $\overline{w}_m$ were ~25% weaker than their respective eyewall counterparts. Of particular note are the $\sigma$ of each region. For eyewalls, the increase with altitude of negative $\overline{w}_m$ within one $\sigma$ of each mean indicates that organized mesoscale downdrafts were more frequent and stronger at midlevels than at low levels. For rainbands, fewer negative $\overline{w}_m$ suggests that appreciable mesoscale downdrafts ($\overline{w}_m < -0.5$ m s$^{-1}$) were less common outside the eyewall.

Figure 7 shows the buoyancy statistics for convective updraft and downdraft cores as a function of altitude in each region. Most mean $\overline{\text{DB}}$ and $\overline{\text{WL}}$ were relatively small and not significantly different from zero at the 95% confidence level (according to a two-tailed $t$ test). As a result, much of the statistically significant vertical structure was captured by the mean $\overline{\text{TB}}$ and $\overline{B}$. Since differences between respective mean $\overline{\text{TB}}$ and $\overline{B}$ are small, only the mean $\overline{B}$ are discussed in detail.

For updraft cores, eyewall mean $\overline{B}$ were slightly positive (~0.1 K) below 4.0 km and near neutral (~0.0 K) above. Rainband mean $\overline{B}$ were positive at all altitudes, increasing to ~0.2 K at 3.0 and 4.2 km, and then decreasing above. Eyewall (rainband) mean $\overline{B}$ at 1.5 and 3.0 km (3.0 and 4.2 km) were significantly different from zero at the 95% level. The larger mean $\overline{B}$ in rainband cores reflect a reduction in background CAPE on approach to the eyewall (Bogner et al. 2000). Moreover, the positive $\overline{B}$ will generate vertical accelerations

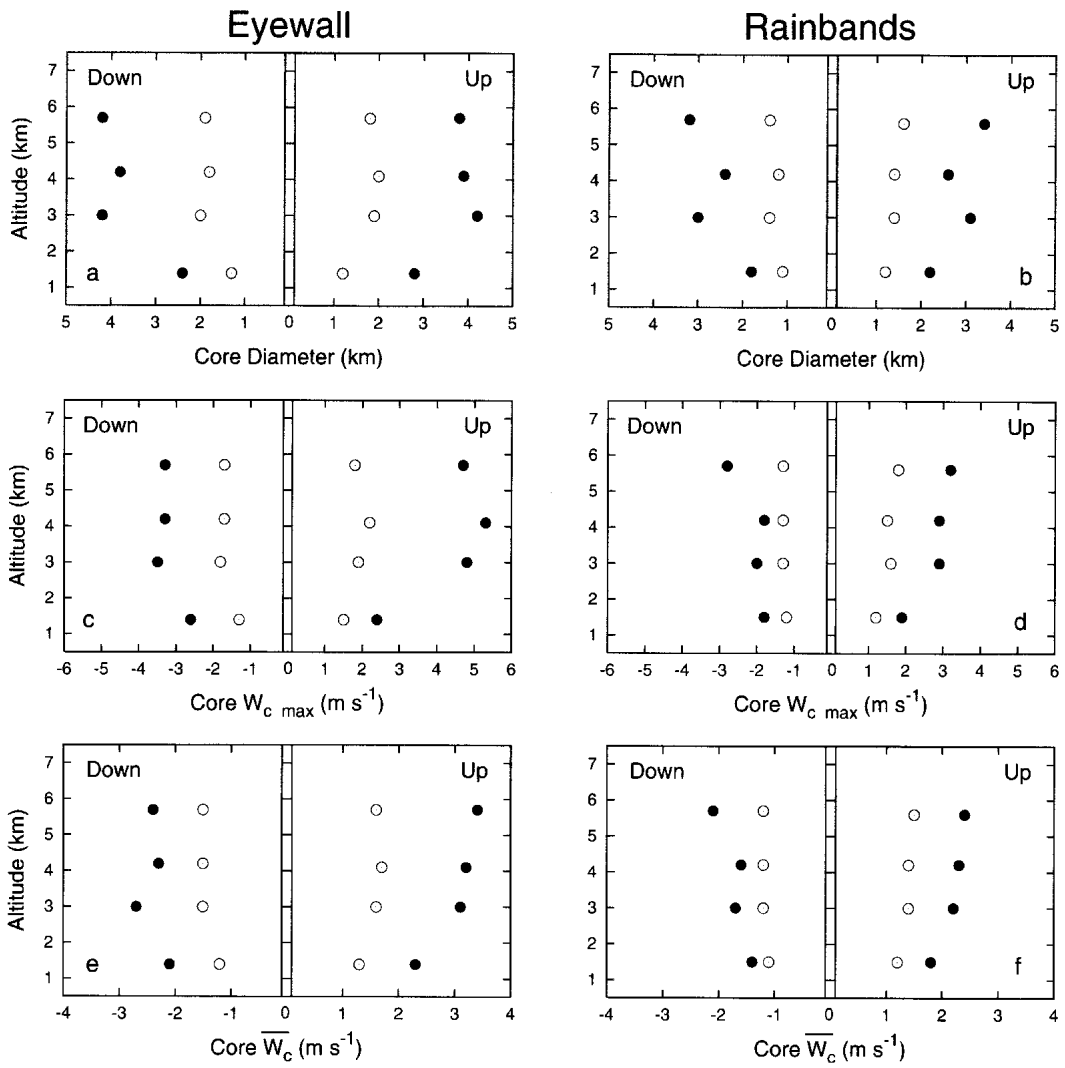


FIG. 5. (top) Variation with altitude of the median (open) and upper 10% level (solid) statistics of diameter DIAM, (middle) maximum convective vertical velocity $w_{c\ \max}$, and (bottom) average convective vertical velocity $\overline{w}_c$ for convective updraft and downdraft cores in the (left) eyewall and (right) rainband regions. The lhs (rhs) of each panel presents the statistics of downdraft (updraft) cores.

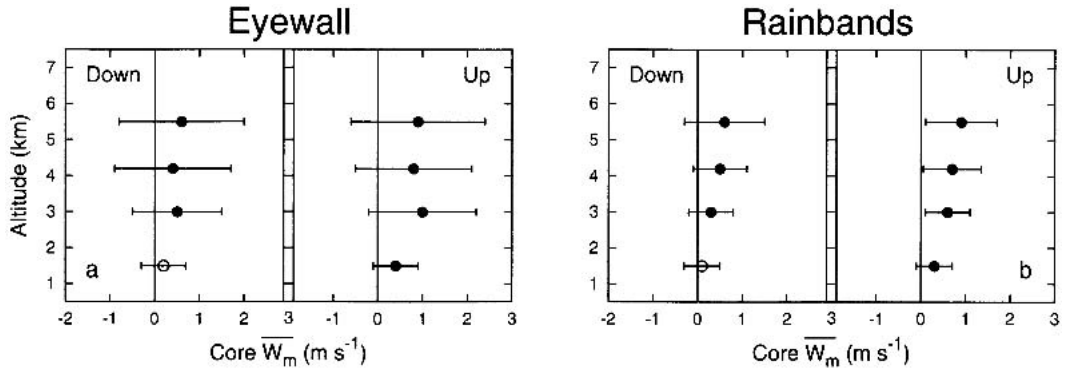


FIG. 6. Variation with altitude of the mean (circles) and standard deviation (bars) of average mesoscale vertical velocity $\overline{w}_m$ for convective updraft and downdraft cores in the (left) eyewall and (right) rainband regions. The lhs (rhs) of each panel presents the statistics of downdraft (updraft) cores. Filled circles denote means significantly different from zero at the 95% level.

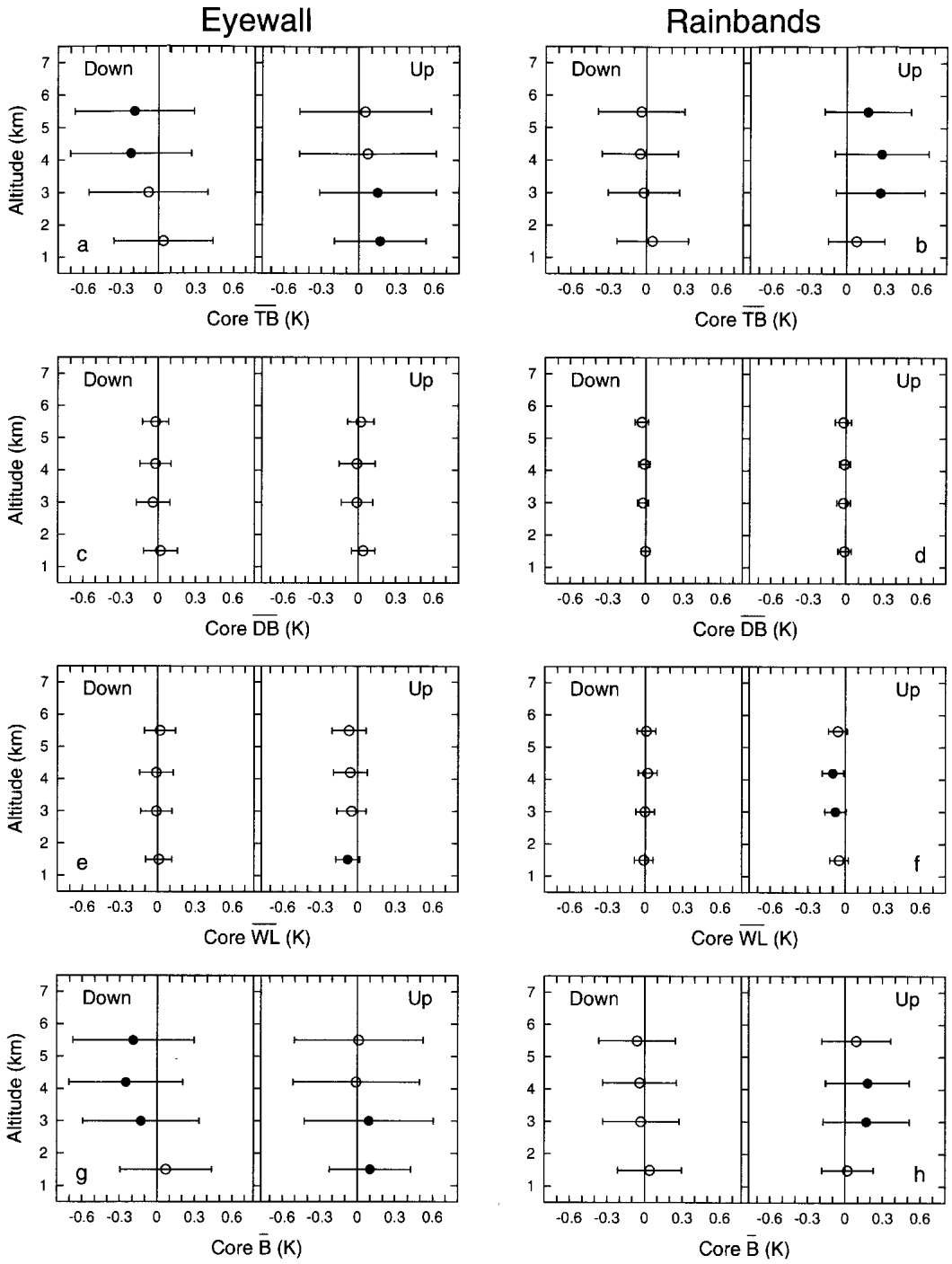


FIG. 7. (top row) Variation with altitude of the mean (circles) and standard deviation (bars) of average thermal buoyancy $\overline{TB}$, (second row) average dynamic buoyancy $\overline{DB}$, (third row) average water loading $\overline{WL}$, and (bottom row) average total buoyancy $\overline{B}$ for convective updraft and downdraft cores in the (left) eyewall and (right) rainband regions. The lhs (rhs) of each panel presents the statistics of downdraft (updraft) cores. Filled circles denote means significantly different from zero at the 95% level.

in updraft magnitude, which is consistent with the updraft core median $\overline{w}_c$ profiles (Figs. 5e,f). We later demonstrate (in section 4a) that such positive $\overline{B}$, despite being small, are entirely adequate to explain the observed increases in $\overline{w}_c$ with altitude for both regions.

For downdraft cores, eyewall mean $\overline{B}$ were negative ($\sim -0.2$ K) at and above 3.0 km, but slightly positive

(~0.1 K) at 1.5 km. Rainband mean $\overline{B}$ exhibited a similar vertical structure but with ~70% smaller magnitudes. Only eyewall mean $\overline{B}$ above 1.5 km were significantly different from zero. The negative $\overline{B}$ suggest that midlevel downdraft cores should accelerate downward, which is qualitatively inconsistent with the median $\overline{w}_c$ profiles (Figs. 5). Such discrepancy is explored further in the next section.

### c. Additional stratifications

Two additional stratifications are presented. The first was motivated by the possibility that an updraft (downdraft) core was superimposed upon mesoscale descent (ascent) of greater magnitude than the core. Such cores will experience heating/cooling processes opposite to those experienced by their counterparts, which may influence the buoyancy statistics. To elucidate any differences, the cores were stratified by their average *total* vertical velocity into two groups: cores that accomplish significant vertical transport ($|\overline{w}| > 1$ m s$^{-1}$) and cores that do not ($|\overline{w}| < 1$ m s$^{-1}$). Over 92% of updraft cores exhibited $\overline{w} > 1$ m s$^{-1}$, and recomputed statistics for these cores (not shown) were nearly identical to those presented in Figs. 3–7. Downdraft cores, however, were evenly distributed between the two groups (~48% exhibited $\overline{w} < -1$ m s$^{-1}$). Statistics were recomputed for both subsets, and significant differences in mean $\overline{B}$ were found (Fig. 8a). For downdraft cores with $\overline{w} < -1$ m s$^{-1}$, mean $\overline{B}$ were slightly positive at all levels, in agreement with studies of ordinary tropical convection (Jorgensen and LeMone 1989; Lucas et al. 1994; Wei et al. 1998). The positive $\overline{B}$ reflect a tendency for adiabatic warming to dominate any evaporational cooling or water loading, which will lead to a deceleration of the downdraft. In contrast, downdraft cores with $\overline{w} > -1$ m s$^{-1}$ exhibit negative median $\overline{B}$ at all levels, which would accelerate the downdrafts, in most cases against the opposing mesoscale updraft. Such differences suggest that many hurricane convective downdraft cores originate as localized regions of negative buoyancy that accelerate downward against mesoscale ascent. Upon overcoming the mesoscale ascent, the downdraft cores can continue to accelerate until adiabatic warming dominates evaporational cooling and water loading (i.e., positive buoyancy is attained), leading to a deceleration and demise of the downdraft.

The second stratification was motivated by the lack of relative humidity and liquid water criteria in the core definition. In particular, are the buoyancy statistics for saturated cores with appreciable liquid water different from subsaturated cores without liquid water? To elucidate any such differences, we separated "moist" cores ($\overline{\text{RH}} > 95\%$ and $\overline{q}_l > 0.05$ g m$^{-3}$) from "dry" cores (either $\overline{\text{RH}} < 95\%$ or $\overline{q}_l < 0.05$ g m$^{-3}$). The thresholds were chosen to account for random instrumental error. We further limited the stratification to cores with $|\overline{w}| > 1$ m s$^{-1}$ in order to eliminate the heating considerations addressed above. Roughly 80% of updraft cores that accomplish significant upward transport were moist. Recomputed statistics for each subset (not shown) revealed no significant differences. In contrast, only ~35% of downdraft cores that accomplish significant downward transport were moist. Recomputed statistics for each subset revealed significant differences in

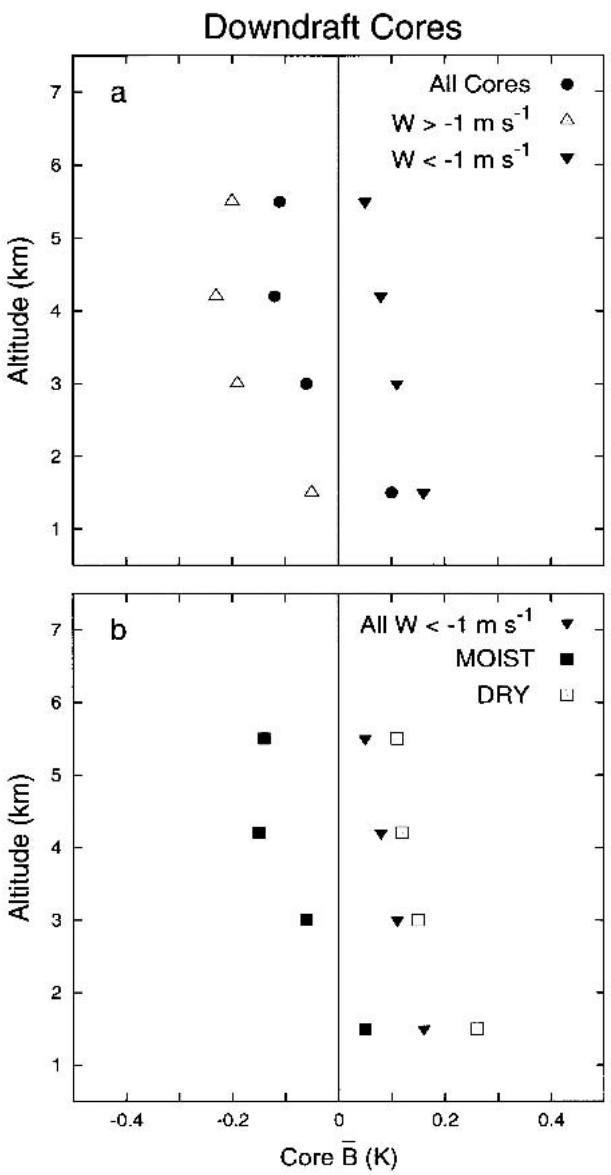


FIG. 8. Variation with altitude of mean average total buoyancy $\overline{B}$ for (a) all convective downdraft cores (filled circles), the subset of downdraft cores with an average total vertical velocity $\overline{w} < -1$ m s$^{-1}$ (filled triangles), and the subset of downdraft cores with $\overline{w} > -1$ ms$^{-1}$ (triangles), and (b) all convective downdraft cores with $\overline{w} < -1$ m s$^{-1}$ (filled triangles) and the further subsets of moist (filled squares) and dry (squares) downdraft cores. Moist cores are defined as having an average relative humidity >95% and total liquid water content >0.05 g m$^{-3}$. Dry cores do not satisfy both criteria. Differences in mean $\overline{B}$ between respective subsets were significant at the 95% level (using a two-tailed *t* test) at all altitudes.

mean $\overline{TB}$, $\overline{WL}$, and $\overline{B}$. Figure 8b shows the mean $\overline{B}$ for each subset. Moist (dry) downdrafts exhibited negative (positive) mean $\overline{B}$ at midlevels. Roughly 75% of the difference was related to $\overline{TB}$ differences, implying that the negative $\overline{B}$ in moist downdraft cores result from evaporative cooling. Betts and Silva Dias (1979) and Srivastava (1987) have demonstrated that negative $\overline{TB}$ can only be maintained over substantial depths (>1 km) if $\overline{q}_l$ exceeds ~4 g m$^{-3}$ or the local lapse rate is nearly dry adiabatic. Since $\overline{q}_l$ rarely exceeds 3 g m$^{-3}$ in hurricanes (Ackerman 1963; Black and Hallett 1986) and inner-core lapse rates are nearly moist adiabatic (Sheets 1969; Frank 1977), the negative $\overline{TB}$ (and $\overline{B}$) are likely short-lived. Thus, adiabatic warming will quickly dominate evaporational cooling and the downdrafts will become subsaturated (i.e., dry downdrafts) and positively buoyant. As a result, downward accelerations are minimized along with core magnitudes. The relatively rarity of moist downdrafts and the overall weak downdraft magnitudes support this assertion.

### *d. Correlations between distributions*

Parcel theory predicts that active cores accelerating upward will have positive $\overline{TB}$ and a positive correlation between $\overline{w}_c$ and $\overline{TB}$. Figure 9 shows scatterplots of $\overline{w}_c$ with respect to $\overline{TB}$ for the updraft cores of each region. In rainbands (Figs. 9c,d), a positive correlation is readily apparent and further illustrated when averages of $\overline{TB}$ are taken over $\overline{w}_c$ intervals; a $\overline{TB}$ of ~0.4 K is

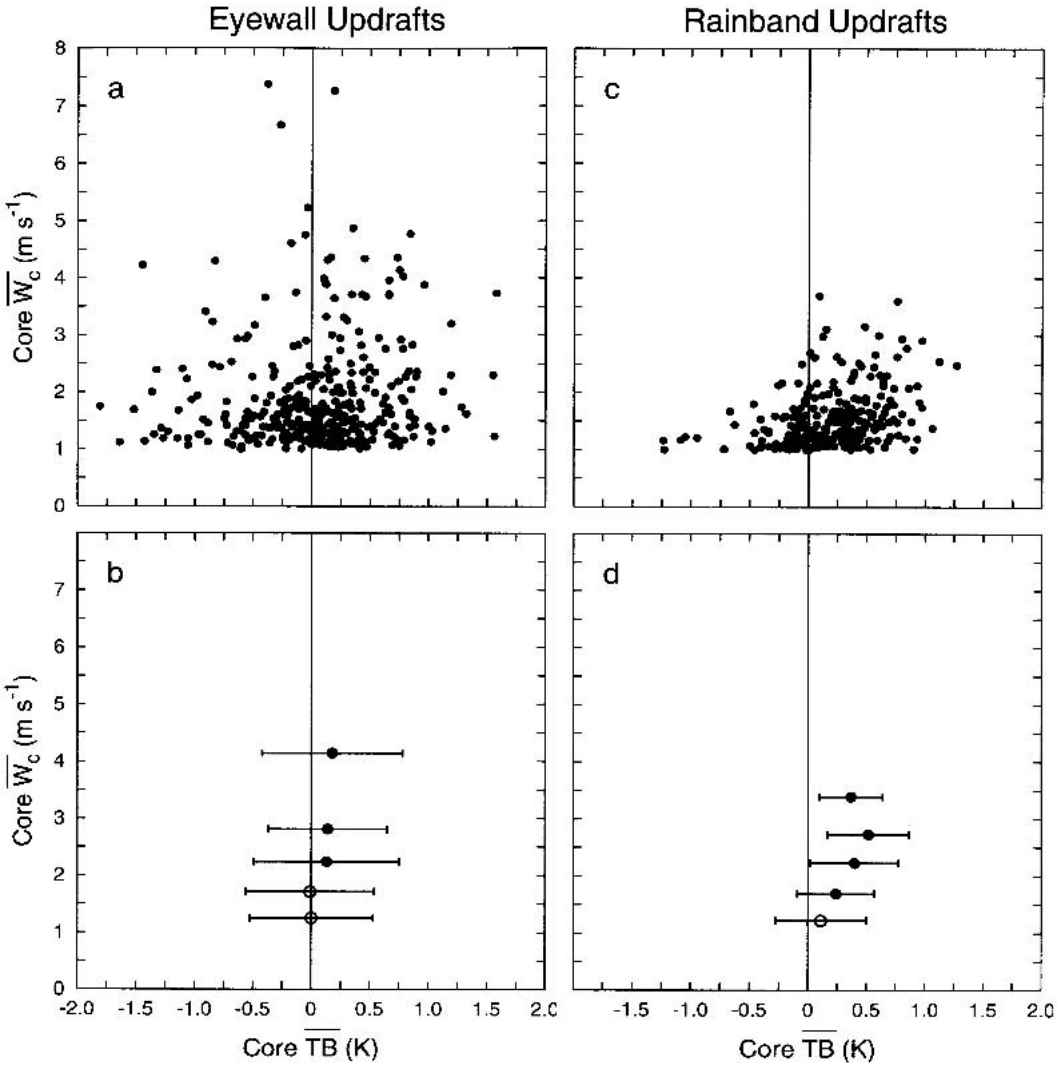


FIG. 9. Scatterplots of convective updraft core average convective vertical velocity $\overline{w}_c$ vs average thermal buoyancy $\overline{TB}$ in the (a) eyewall and (c) rainband regions. Means (circles) and standard deviations (bars) of $\overline{TB}$ taken over specified $\overline{w}_c$ intervals for the (b) eyewall and (d) rainband cores. Filled circles denote means significantly different from zero at the 95% level. The vertical velocity intervals used were $1.0 < \overline{w}_c < 1.5$ m s$^{-1}$, $1.5 < \overline{w}_c < 2.0$ m s$^{-1}$, $2.0 < \overline{w}_c < 2.5$ m s$^{-1}$, $2.5 < \overline{w}_c < 3.0$ m s$^{-1}$, and $\overline{w}_c > 3.0$ m s$^{-1}$.

representative for the stronger ($\overline{w}_c > 2$ m s$^{-1}$) updraft cores. In the eyewall (Figs. 9a,b), a weak positive correlation is only apparent after averaging $\overline{\text{TB}}$ over $\overline{w}_c$ intervals; a $\overline{\text{TB}}$ of ~0.2 K is representative for the stronger updraft cores.

Table 2 shows linear correlation coefficients of $\overline{w}_c$ with $\overline{\text{TB}}$, DIAM with $\overline{\text{TB}}$, and $\overline{w}_c$ with DIAM for both updraft and downdraft cores as a function of altitude and region. For updraft cores, weak positive correlations exhibit an increase with altitude that becomes significant at the 95% level (according to a two-tailed *t* test) by 5.5 km (4.2 km) in the eyewall (rainband) region. Such an increase suggests that a greater fraction of the large and strong midlevel updraft cores are more buoyant than their low-level counterparts. Downdraft cores exhibit no significant or systematic relationship between $\overline{\text{TB}}$ and either $\overline{w}_c$ or DIAM at any level. The overall weakness of the correlations is striking. Recall, however, that our data represent a random sample of growing, mature, and dissipating convection undergoing continuous entrainment (which is neglected or assumed minimal in parcel theory).

### e. Area occupied by convective cores

The fractional area occupied by convective cores with certain vertical velocity or buoyancy characteristics with an intense hurricane can be estimated from the fraction of the radial legs occupied by such cores since the azimuthal distribution of legs was fairly uniform and independent of a given storm's azimuthal convective structure. Following JZL, we first compute the fractional area of each convective core as

$$\text{FA} = \pi \frac{r_{\text{out}}^2 - r_{\text{in}}^2}{R_{\text{out}}^2 - R_{\text{in}}^2}, \tag{3}$$

where $r_{\text{in}}$ and $r_{\text{out}}$ are the inner and outer edge radii of the core, and $R_{\text{in}}$ and $R_{\text{out}}$ are the inner and outer radial extents of the region (eyewall, rainband, or entire leg). The percent area coverage was computed by summing the FA of each core encountered during a given leg and then averaging over all legs. The mean radial leg extends from ~15 to ~115 km with a mean radial cutoff between the eyewall and rainband region at ~45 km.

Convective updraft and downdraft cores occupied 4% and 3% of the total area inside 115 km, respectively. JZL estimated that their updraft and downdraft cores occupied 9% and 4% of the area inside 137 km. Despite differences in core definition, data resolution, and total area, the consistent results imply that a relatively small area of the hurricane inner core is covered by meaningful convective-scale vertical motions. Similar conclusions were reached by Malkus et al. (1961), Marks (1985), and Black et al. (1996) using radar data.

Figure 10 shows the cumulative percentage of the eyewall and rainband region occupied by convective updraft and downdraft cores with $\overline{w}_c$ and $\overline{B}$ greater than the values indicated. For example, updraft cores occupied 9.9% of the total eyewall area, but updrafts with *either* $\overline{w}_c > 2$ m s$^{-1}$ *or* $\overline{B} > 0$ K occupied only ~5% of the same area. In the rainband region, updraft cores covered only 2.9% of the total area, with ~2.5% of the area occupied by buoyant ($\overline{B} > 0$ K) updrafts. Downdraft cores occupied only 9.2% of the eyewall area and only 2.3% of the the rainband area.

### f. Vertical mass transport by convective updraft cores

To estimate the convective updraft core contribution to the total upward mass transport, we first follow JZL and compute a convective mass transport per unit length normal to the flight track for each core as

$$\text{MT}_c = \rho \overline{w}_c \text{DIAM}, \tag{4}$$

where $\rho$ is the density of air, and $\overline{w}_c$ and DIAM are defined as before. The net convective contribution was then estimated by summing the $\text{MT}_c$ of each updraft core encountered over all legs. Only updraft cores with $\overline{w} > 1$ m s$^{-1}$ were included. Next, the total upward mass transport per unit length normal to the flight track along each leg was computed as

$$\text{MT} = \rho \overline{w}_{\text{leg}} \text{L}, \tag{5}$$

where $\overline{w}_{\text{leg}}$ is the mean total upward vertical velocity along the leg, and L is the leg length. The net total transport was then computed by summing the leg MT

TABLE 2. Linear correlation coefficients between average convective vertical velocity $\overline{w}_c$, average thermal buoyancy $\overline{\text{TB}}$, and diameter DIAM for convective updraft and downdraft cores in the eyewall and rainband regions. Coefficients for downdraft cores are shown in parentheses. Values in boldface are significantly different from zero at the 95% level.

| Region | Altitude (km) | No. of cores | Linear correlation coefficients | | |
|---|---|---|---|---|---|
| | | | $\overline{w}_c$–$\overline{\text{TB}}$ | DIAM–$\overline{\text{TB}}$ | $\overline{w}_c$–DIAM |
| Eyewall | 5.5 | 115 (119) | **0.33** (−0.20) | **0.26** (−0.18) | **0.57 (−0.51)** |
| | 4.2 | 72 (85) | 0.08 (−0.01) | 0.07 (−0.01) | **0.54 (−0.57)** |
| | 3.0 | 127 (131) | 0.01 (0.11) | −0.07 (−0.09) | **0.57 (−0.55)** |
| | 1.5 | 37 (34) | 0.02 (0.20) | 0.03 (0.04) | 0.24 **(−0.35)** |
| Rainband | 5.5 | 66 (50) | **0.46** (−0.20) | 0.16 (−0.14) | **0.53 (−0.77)** |
| | 4.2 | 68 (47) | **0.59** (0.19) | **0.39** (0.13) | **0.70 (−0.64)** |
| | 3.0 | 105 (86) | **0.19** (−0.10) | 0.09 (−0.03) | **0.65 (−0.62)** |
| | 1.5 | 30 (18) | 0.03 (−0.21) | 0.30 (−0.16) | **0.47 (−0.58)** |

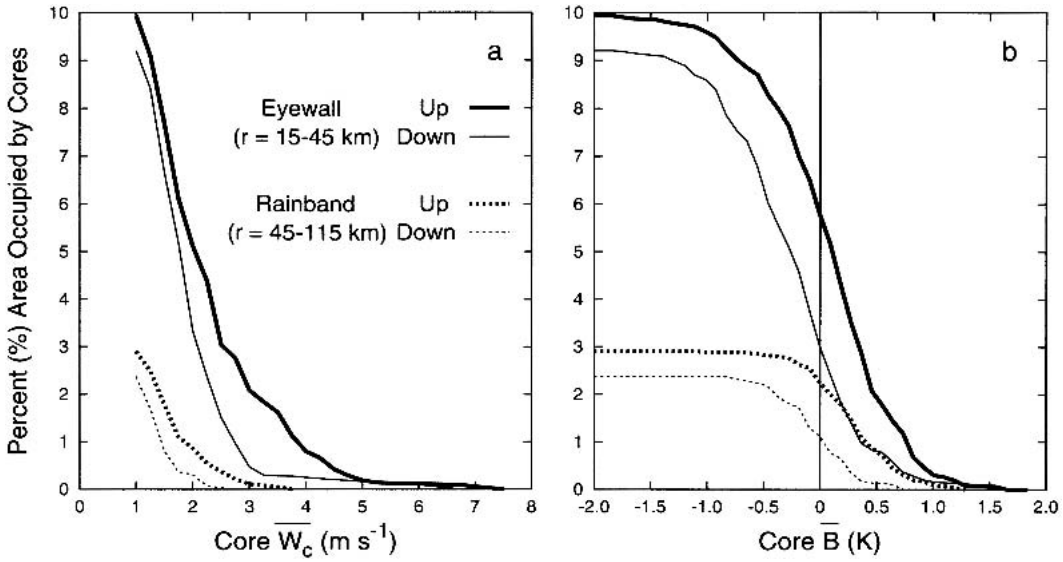


FIG. 10. Cumulative percentage of the eyewall (solid) and rainband (dotted) region occupied by convective updraft (thick lines) and downdraft (thin lines) cores with (a) average convective vertical velocities $\overline{w}_c$ and (b) average total buoyancies $\overline{B}$ greater than the magnitude given on the abscissa.

over all legs. Finally, the percent total upward mass transport by the updraft cores was estimated by dividing the $MT_c$ net contribution by the MT net transport.

Figure 11 shows the cumulative percentage of total upward mass transport accomplished by convective updraft cores as a function of $\overline{w}_c$ and $\overline{B}$ greater than the values indicated. Updraft cores accomplished ~64% and ~51% of the total upward mass transport in the eyewall and rainband regions, respectively. Moreover, updraft cores with *either* $\overline{w}_c > 2$ m s$^{-1}$ *or* $\overline{B} > 0$ K (which occupied <5% of the area) accomplished ~30%–40% of the total upward transport in each region. Updraft cores with *both* $\overline{w}_c > 2$ m s$^{-1}$ *and* $\overline{B} > 0$ K (only 16% of all updrafts) occupied < 2% of the total area but accomplished ~25% of the total transport. Clearly localized buoyant updraft cores make a consid-

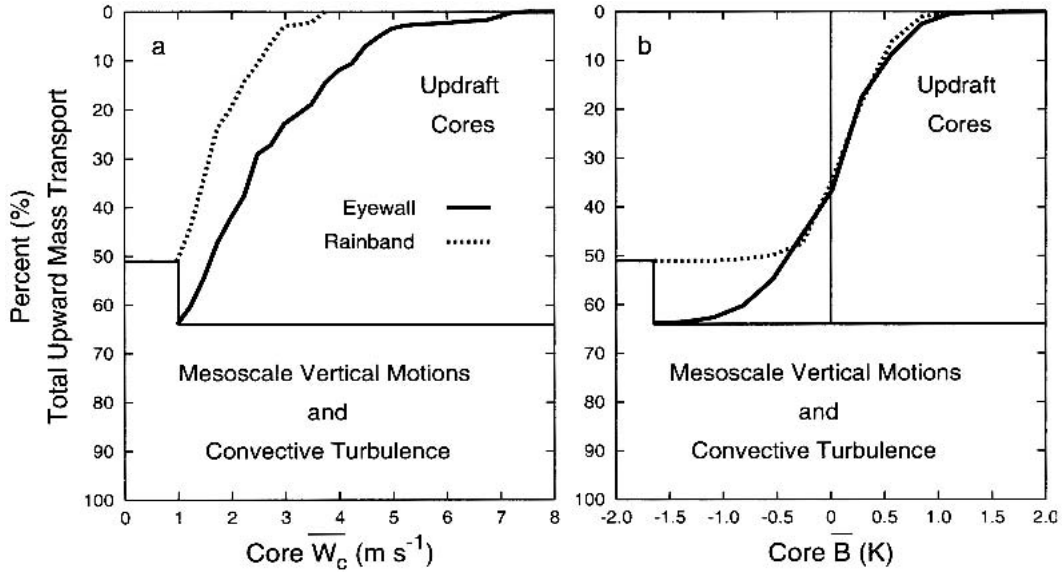


FIG. 11. Cumulative percentage of the total upward mass transport accomplished by eyewall (solid) and rainband (dotted) convective updraft cores with (a) average convective vertical velocities $\overline{w}_c$ and (b) average total buoyancies $\overline{B}$ greater than the magnitude given on the abscissa. The percentage of total upward mass transport accomplished by mesoscale updrafts and convective turbulence in each region lies below the horizontal lines.

erable contribution to the total mass transport in the hurricane inner core.

## 4. Discussion

### a. Vertical acceleration of ordinary convective updraft cores

Zhang et al. (2000) examined the inner-core vertical momentum budget using azimuthally and temporally (over 1 h) averaged output from an explicit three-dimensional hurricane simulation with 6-km horizontal grid spacing and found the mean eyewall to be moist neutral to a first approximation. Small vertical accelerations in the mean eyewall updraft above the boundary layer were attributed to upward-directed perturbation pressure gradient forces. Recently, Braun (2002) examined the vertical momentum budget along individual eyewall updraft trajectories using 2-min output from an explicit three-dimensional hurricane simulation with 1.3-km horizontal grid spacing. In contrast to Zhang et al. (2000), perturbation pressure gradient forces were directed downward and positive total buoyancy forces were argued to drive the modest updraft accelerations found above the boundary layer. Therefore, these studies suggest that while the azimuthally averaged eyewall may be neutral or negatively buoyant with minimal updraft acceleration, individual convective updrafts may exhibit appreciable positive buoyancy and upward acceleration.

What do the observations of "ordinary" convective updraft cores suggest? The median $\overline{w}_c$ for eyewall and rainband updrafts exhibited a slight increase in strength with altitude (i.e., an acceleration) above the boundary layer. Updraft mean $\overline{B}$ were also significantly positive below ~4 km (between ~2–5 km) in eyewalls (rainbands), suggesting that ordinary updraft core accelerations may result from appreciable positive buoyancy forces.

We can elucidate the *relative* roles played by total buoyancy and the perturbation pressure gradient force in vertically accelerating hurricane updraft cores through a rough calculation with a one-dimensional updraft model. In the absence of lateral forcing or entrainment mixing, the convective vertical momentum equation can be written as

$$\frac{dw_c}{dz} = \frac{1}{w_c}\left(\frac{1}{\rho}\frac{dp'}{dz} + B\right), \tag{6}$$

where $\overline{w}_c$, $\rho$, $p'$, and $B$ are defined as before, and the first term inside the bracket is the vertical perturbation pressure gradient force (VPPGF). We apply to Eq. (6) the median statistics from each region in order to capture the behavior of an ordinary updraft core. In other words, we assume the buoyancy of an ordinary updraft evolves with altitude as the median $\overline{B}$ profile evolves.[3] Unfortunately, observational estimates of the VPPGF are beyond the capabilities of current instrumentation. Therefore, we use Eq. (6) to derive profiles of expected updraft core $\overline{w}_c$ forced from $B$ alone, and then infer the relative VPPGF from the difference between the expected and observed $\overline{w}_c$ profiles. Expected $\overline{w}_c$ profiles are determined through upward integration of Eq. (6) using the median $\overline{w}_c$ at 1.5 km as the lower boundary condition. Clearly this simple model has shortcomings, but a more sophisticated treatment is not justified without detailed observational knowledge of the local three-dimensional environment in which the updraft cores rise.

Figure 12 shows the profiles of observed and expected median $\overline{w}_c$ for eyewall and rainband updraft cores. In both regions, the expected $\overline{w}_c$ from $\overline{B}$ alone exhibit substantially more vertical acceleration than observed, resulting in updrafts 4–5 m s$^{-1}$ stronger at 5.5 km. Note that the expected eyewall $\overline{w}_c$ also exhibits a weak deceleration above 4.2 km (due to a negative median $\overline{B}$ at 4.2 km) in agreement with the observations. Inferring the VPPGF as the residual, the profiles suggest that an ordinary VPPGF acting upon an updraft core is directed downward and largely opposes the positive buoyancy force. The results further imply that buoyancy is the primary force vertically accelerating the eyewall and rainband updraft cores above the boundary layer. Such findings are consistent with Braun (2002).

The relative roles of $\overline{\text{WL}}$ and $\overline{\text{DB}}$ can also be elucidated through comparison of the expected $\overline{w}_c$ from $\overline{B}$ with the expected $\overline{w}_c$ from integrating Eq. (6) with the median $\overline{\text{TB}}$ statistics (see Fig. 12). In both regions, the expected $\overline{w}_c$ from $\overline{\text{TB}}$ are 1–2 m s$^{-1}$ stronger than their $\overline{w}_c$ from $\overline{B}$ counterparts; ~80% of the difference is due to $\overline{\text{WL}}$. Therefore, $\overline{\text{WL}}$ (as expected) and $\overline{\text{DB}}$ (to a lesser degree) act to decelerate ordinary updrafts.

The effects of entrainment mixing were neglected in the updraft model for simplicity. We can, however, assume that the *net* effects of entrainment are implicit within the median $\overline{w}_c$ and $\overline{\text{TB}}$ statistics at each level. Therefore, the effects of entrainment on ordinary updraft accelerations can be inferred through a comparison of the expected $\overline{w}_c$ from $\overline{\text{TB}}$ with the expected $\overline{w}_c$ derived from median TB statistics for *undilute* moist ascent. Representative estimates of undilute TB were obtained from 223 GPS dropwindsondes (Hock and Franklin 1999) deployed in the inner core of eight intense hurricanes (Table 3). The soundings were acquired from the NOAA HRD quality-controlled data archive and further scrutinized, following Bogner et al. (2000), to correct any mixed-layer humidity-sensor wet-

[3] Median $\overline{\text{TB}}$, $\overline{\text{DB}}$, $\overline{\text{WL}}$, and $\overline{B}$ values were nearly identical to the means shown in Fig. 7 at each altitude in both regions (Eastin 2003).

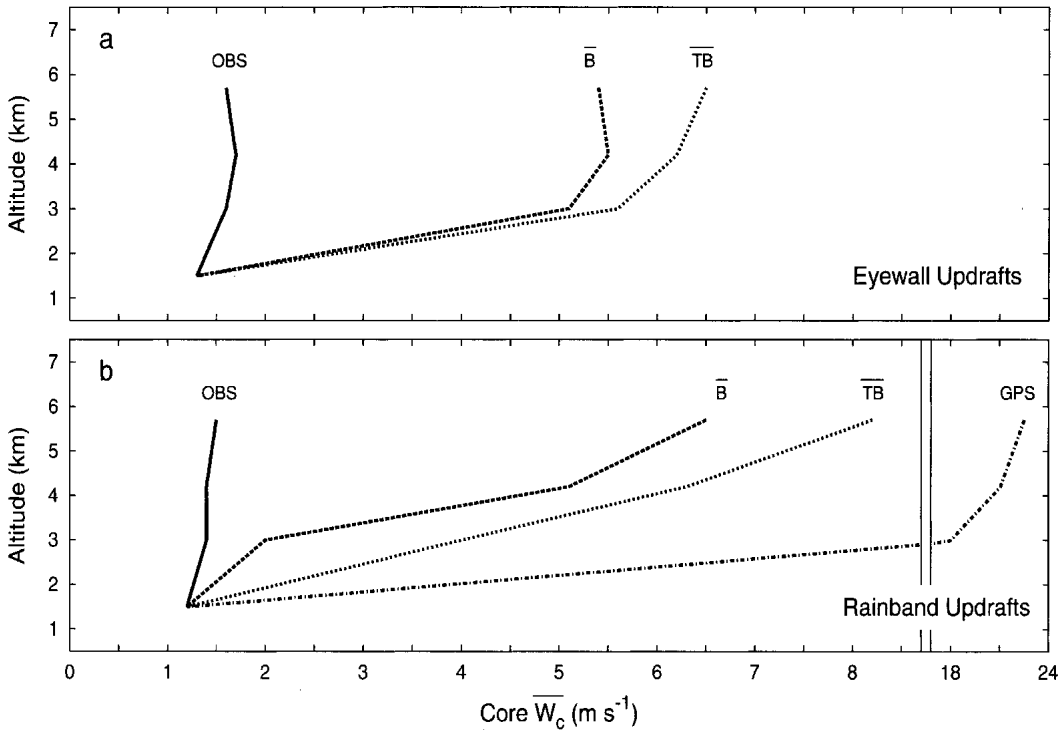


FIG. 12. Variation with altitude of the observed (a) eyewall and (b) rainband convective updraft core median average convective vertical velocity $\overline{w}_c$ (OBS; solid) and the $\overline{w}_c$ values expected from parcel theory [Eq. (6)] using the median values of core average total buoyancy ($\overline{B}$; dashed), core average thermal buoyancy ($\overline{\text{TB}}$; dotted), and thermal buoyancy derived from GPS dropsondes assuming undilute moist-adiabatic ascent of the lowest 500 m (GPS; dot–dash).

ting errors.[4] Next, the soundings were subjectively stratified by region using methods consistent with the convective core stratification. Vertical profiles of undilute TB were then calculated for each sounding as the difference in $\theta_v$ between a parcel lifted pseudoadiabatically from the boundary layer and the observed sounding. The lifted parcel was characterized by the mean conditions in the lowest 500 m. Finally, undilute TB values were extracted from the profiles at each available reference altitude and tabulated.

Figure 13 shows the updraft core median $\overline{\text{TB}}$ and undilute parcel median TB for each region. Also shown for comparison are the undilute TB computed from the Frank (1977) composite typhoon sounding at ~80 km radius. In the rainband region (Fig. 13b), both undilute profiles indicate that ordinary updraft cores should exhibit $\overline{\text{TB}} > 1.0$ K at 4.2 km, rather than the 0.24 K observed. Clearly entrainment reduced core $\overline{\text{TB}}$ values. The net effect on updraft acceleration is illustrated in Fig. 12b. Entrainment effectively reduced $\overline{w}_c$ at 5.5 km by ~14 m s$^{-1}$, which was more than either WL (~2 m s$^{-1}$) or the VPPGF (~5 m s$^{-1}$). In the eyewall region (Fig. 13a), median undilute TB are near neutral (~0.02 K) and *less* than the updraft core $\overline{\text{TB}}$ values. Since the GPS soundings collectively provide a mesoscale representation of the quasi-vertical structure, this result supports the idea that buoyant convective updrafts are embedded within a near-neutral mesoscale eyewall. Evidence of detrimental entrainment is limited to the slight decrease in core $\overline{\text{TB}}$ with altitude. Less entrainment in the eyewall would not be surprising. Helfrich (1994) and Ayotte and Fernando (1994) have demonstrated experimentally that thermals ascending in rapidly rotating environments experience less lateral entrainment than their counterparts in nonrotational environments.

The fact that condensate freezing can invigorate an updraft ascending above the 0°C level is well known (Riehl 1979; Zipser 2003). Note that updraft core mean $\overline{B}$ above ~4 km (Fig. 7) exhibited either neutral conditions or a marked trend toward negative buoyancy, which would limit further core ascent in the absence of mesoscale forcing. However, if a near-neutral updraft core contained ~0.5 g m$^{-3}$ of liquid water upon reaching the freezing level (typical for hurricane updrafts; JZL), total condensate freezing would reinvigo-

[4] Humidity-sensor wetting errors may still exist above the mixed layer. Such errors will result in an overestimate of humidity, and thus an underestimate of undilute TB. The errors are probably somewhat balanced by a known dry bias (Wang et al. 2002).

TABLE 3. Summary of GPS dropwindsonde data used in this study.

| Storm | Date yr/mo/day | Storm intensity (mb) | Flight ID | Flight Altitude (km) | No. of GPS sondes Eyewall region | No. of GPS sondes Rainband region |
|---|---|---|---|---|---|---|
| Guillermo | 97/08/02 | 950 | I | 5.5 | — | 9 |
| | 97/08/03 | 923 | H | 3.0 | 6 | — |
| | | | I | 5.5 | — | 5 |
| Erika | 97/09/08 | 950 | I | 2.5 | 9 | 6 |
| Bonnie | 98/08/23 | 955 | A | 3.0 | 1 | — |
| | | | H | 5.5 | 4 | 7 |
| | | | I | 4.2 | 1 | 4 |
| | 98/08/24 | 962 | A | 3.0 | — | 1 |
| | | | H | 4.2 | 1 | 12 |
| | 98/08/26 | 963 | A | 3.0 | — | 2 |
| | | | H | 4.2 | 5 | 17 |
| | | | I | 2.0 | 2 | 8 |
| Georges | 98/09/19 | 939 | A | 3.0 | 1 | — |
| | | | H | 4.2 | 6 | 5 |
| | | | I | 4.2 | 7 | 6 |
| | 98/09/20 | 941 | A | 3.0 | 3 | — |
| | 98/09/21 | 965 | A | 3.0 | 1 | — |
| | 98/09/22 | 965 | A | 3.0 | 1 | 4 |
| Mitch | 98/10/25 | 950 | A | 3.0 | 3 | — |
| | 98/10/26 | 916 | A | 3.0 | 5 | — |
| | 98/10/27 | 925 | A | 3.0 | 5 | — |
| | | 928 | I | 3.0 | 20 | 3 |
| | 98/10/28 | 942 | A | 3.0 | 3 | — |
| Bret | 99/08/22 | 949 | A | 3.0 | 3 | — |
| Floyd | 99/09/12 | 955 | A | 3.0 | 8 | — |
| | 99/09/13 | 922 | A | 3.0 | 6 | — |
| | | | I | 3.0 | 4 | 6 |
| | 99/09/14 | 929 | A | 3.0 | 3 | — |
| | 99/09/15 | 940 | A | 3.0 | 5 | — |
| Lenny | 99/11/16 | 962 | A | 3.0 | 4 | — |
| | 99/11/17 | 949 | A | 3.0 | 6 | — |
| | 99/11/18 | 952 | A | 3.0 | 4 | 1 |
| Total | | | | | 127 | 96 |

rate the updraft with ~0.3 K of $\overline{TB}$ and buoyant ascent could continue. Of the updraft cores at 5.5 km, roughly 35% were encountered at temperatures <0°C. The mean $\overline{TB}$ of these cores was more positive than the mean $\overline{TB}$ of the warmer cores at 5.5 km, but the difference in means was not statistically significant. Nevertheless, observed hurricane updrafts are stronger above the freezing level (Marks and Houze 1987; Black et al. 1996), suggesting that condensate freezing plays a substantial role in maintaining positive buoyancy and upward accelerations against entrainment, water loading, and downward-directed pressure gradient forces.[5] Such arguments are consistent with the modeling results of Lord et al. (1984).

### b. *Are buoyant convective updraft cores "hot towers"?*

Two contrasting conceptual theories concerning the role of buoyancy in hurricane convection have been put forth. First, Malkus and Riehl (1960) speculated that a large fraction of the mass lifted from the surface to upper levels ascends rapidly in a few *undilute* buoyant updrafts, or "hot towers," rather than gradually in a symmetric mesoscale updraft. Their hypothesis was supported by symmetric mass and energy budgets for Hurricane Daisy (1958; Riehl and Malkus 1961) and by radar and photographic cloud analyses (Malkus et al. 1961). In contrast, Emanuel (1986) argued that the hurricane inner core is often close to a state of moist symmetric neutrality in which moist enthalpy and angular momentum surfaces correspond. As a result, the vertical mass transport is accomplished by uniform rings of mesoscale ascent forced entirely by boundary layer convergence with a *negligible* contribution from buoyancy. His hypothesis was supported by the decrease in CAPE on approach to the eyewall (Frank 1977) and idealized numerical simulations (Rotunno and Emanuel 1987).

What do our results suggest? The presence of numerous convective-scale buoyant updraft cores, superimposed upon mesoscale currents of rising air, that occupy only a small fraction of the total area but accomplish a

[5] Precipitation fallout will also contribute to updraft acceleration above the freezing level.

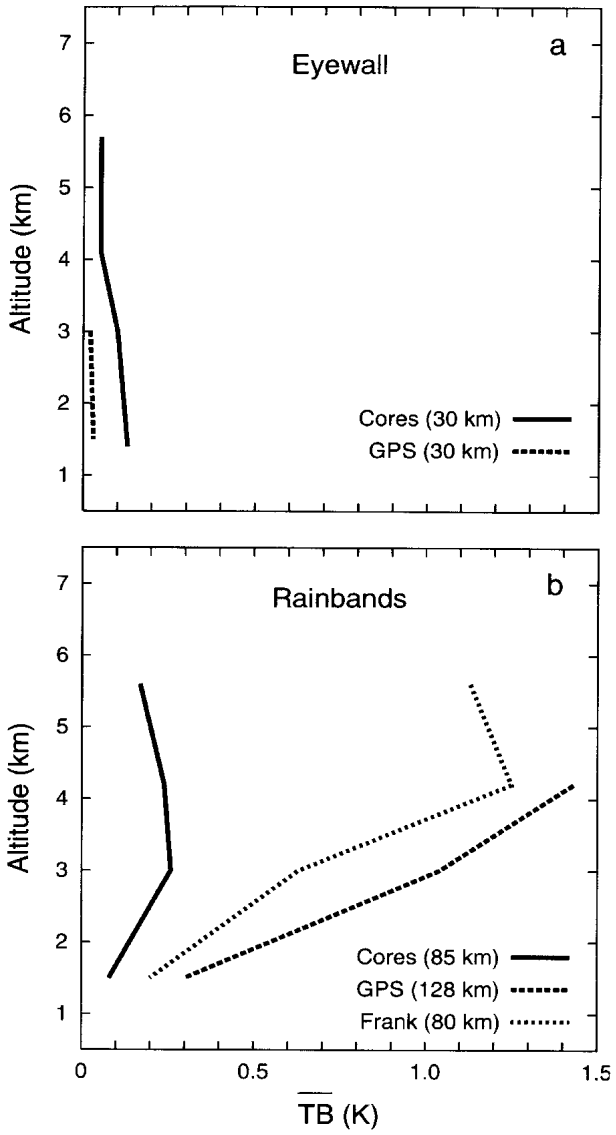


FIG. 13. Variation with altitude of the observed (a) eyewall and (b) rainband convective updraft core median average thermal buoyancy $\overline{TB}$ (solid) and the median TB derived from GPS dropsondes (dashed) deployed in each region (127 eyewall sondes; 96 rainband sondes) assuming undilute moist-adiabatic ascent of the lowest 500 m. Shown for comparison in the rainband region are the TB derived from the Frank (1977) composite typhoon sounding at $r = 80$ km assuming undilute moist-adiabatic ascent of the lowest 50 mb (dotted). Values in parentheses are the mean radii of the cores or soundings used to determine the median values in each region. GPS-derived median values are only shown at levels with at least 30 individual estimates in order to ensure an adequate statistical sample.

considerable fraction of the vertical mass transport qualitatively support the hot tower concept. However, the overall small positive mean $\overline{B}$; weak correlations between $\overline{B}$, $\overline{w}_c$, and DIAM; and evidence of considerable entrainment contradict the hot tower hypothesis. Clearly the vast majority of buoyant convective updraft cores are not the envisioned hot towers. The same results also suggest that moist symmetric neutrality is not strictly valid. How then might our results be interpreted? The observations suggest that *an ensemble of buoyant convective updrafts is a significant component of the transverse circulation* and may play an integral role in hurricane maintenance and evolution.

## 5. Summary and conclusions

Aircraft data from 25 flights into 14 intense hurricanes have been used to derive kinematic and buoyancy statistics for convective-scale vertical velocity events, called cores, superimposed upon the mesoscale transverse circulation. Initially, all data were filtered to effectively separate the balanced mesoscale structure from the potentially unbalanced convective-scale structure in a manner consistent with both observations and current theory. Cores were defined as flight-leg segments in which the convective-scale vertical velocity ($w_c$) exceeded an absolute value of 1 m s$^{-1}$ for at least 0.5 km. The total buoyancy ($B$) was defined from convective-scale virtual potential temperature, pressure, and liquid water content assuming the respective mesoscale fields represent the appropriate reference state. Statistics of core kinematic and buoyancy properties have been summarized for the eyewall and inner rainband regions at four altitude levels from 1.5 to 5.5 km. Our findings reveal the following:

1) Distributions of convective core diameter, maximum $w_c$, and average $w_c$ were approximately lognormal. Over 90% of cores were <4 km in diameter and <4 m s$^{-1}$ in average magnitude. The upper 10% of eyewall cores were both larger (by ~1 km) and stronger (by 1–2 m s$^{-1}$ for average $w_c$) than corresponding rainband cores. The results are consistent with previous studies (JZL; Black et al. 1996) despite different core criteria.
2) Distributions of core average mesoscale vertical velocity were approximately normal with mean values of ~0.5 m s$^{-1}$ for both updrafts and downdrafts. Most cores were superimposed upon mesoscale ascent. In the eyewall, however, ~35% were superimposed upon mesoscale downdrafts, which suggests that hurricane eyewalls are not quasi-symmetric rings of ascent but contain regions of organized mesoscale descent.
3) Both eyewall and rainband convective updraft cores exhibited a ~0.5 m s$^{-1}$ increase in median average $w_c$ over altitudes between 1.5 and 5.5 km, which implies that ordinary updraft cores experience a modest upward acceleration above the boundary layer. Downdraft cores in each region tended to be stronger at midlevels than at low levels.
4) Most convective updraft cores in the eyewall (~54%) and rainband (~63%) regions exhibited positive total buoyancy. For the mean eyewall up-

draft, statistically significant positive average $B$ of ~0.1 K were found at altitudes below 4 km, with near-neutral values above. The mean rainband updraft exhibited significant positive average $B$ of ~0.2 K at altitudes between 2 and 5 km. Regional differences are consistent with a reduction in background CAPE on approach to the eyewall (Frank 1977; Bogner et al. 2000).

5) Convective downdraft cores not superimposed upon stronger mesoscale updrafts (i.e., cores that transport mass downward) tended to exhibit positive average $B$ at all altitudes, particularly the subsaturated cores with minimal liquid water content. The results suggest that downdraft cores are more transient than updraft cores.
6) Convective updraft cores occupied <10% of the eyewall region (annulus between ~15 and ~45 km radius) but accomplished ~65% of the total upward mass transport. Buoyant updraft cores covered <5% of the same area but accomplished ~40% of the total transport. Similar results were found for the rainband region.
7) Application of the median statistics from each region to a one-dimensional updraft model indicated that an ordinary updraft core average $B$ was more than adequate to explain the observed increase in core strength with altitude. The results imply that ordinary vertical perturbation pressure gradient forces are directed downward and oppose positive buoyancy forces. Entrainment and water loading were also found to substantially reduce updraft core magnitudes.
8) The observations support some aspects of both the hot tower hypothesis (Malkus and Riehl 1960) and symmetric moist neutral ascent (Emanuel 1986), but neither concept appears dominant. While convective updraft cores occupy a small fraction of the eyewall and account for most of the vertical mass transport, the updrafts are more numerous and much weaker, in terms of both vertical velocity and buoyancy, than those envisioned when the hot tower hypothesis was first advanced. Buoyant convective updrafts, however, appear to be integral components of the transverse circulation.

A companion paper (Eastin et al. 2004) examines case studies of two hurricanes in order to illustrate the azimuthal distribution of buoyant convection, demonstrate that the low-level eye can be an important source region for buoyant eyewall convection, and provide evidence of three physical links between buoyant convection and hurricane evolution.

*Acknowledgments.* The authors are indebted to the scientists and flight crews from NOAA's HRD and Aircraft Operations Center for their dedicated efforts over the past two decades to collect the data used in this study. We wish to thank Hugh Willoughby and Ed Rahn for developing the processed radial leg database; Frank Marks and Paul Leighton for providing the along-track reflectivity profiles; and James Franklin, Mike Black, and Steve Feuer for providing the GPS dropsonde data. We are grateful to Ed Zipser, Frank Marks, and Jim Kossin for insightful discussions regarding this work. Constructive comments by Mike Montgomery, Wayne Schubert, Mike Black, and one anonymous reviewer were also very beneficial. This research was supported by NSF Grants ATM-0071369 and ATM-9616818.

## REFERENCES

Ackerman, B., 1963: The distribution of liquid water in hurricanes. National Hurricane Research Project Rep. 62, U.S. Weather Bureau, 41 pp.

Ayotte, B. A., and H. J. S. Fernando, 1994: The motion of a turbulent thermal in the presence of background rotation. *J. Atmos. Sci.,* **51,** 1989–1994.

Barnes, G. M., E. J. Zipser, D. Jorgensen, and F. Marks Jr., 1983: Mesoscale and convective structure of a hurricane rainband. *J. Atmos. Sci.,* **40,** 2127–2137.

Baumgardner, D., 1983: An analysis and comparison of five water droplet measuring devices. *J. Climate Appl. Meteor.,* **22,** 891–910.

Betts, A. K., and M. F. Silva Dias, 1979: Unsaturated downdraft thermodynamics in cumulonimbus. *J. Atmos. Sci.,* **36,** 1061–1071.

Black, M. L., R. W. Burpee, and F. D. Marks Jr., 1996: Vertical motion characteristics of tropical cyclones determined with airborne Doppler radial velocities. *J. Atmos. Sci.,* **53,** 1887–1909.

Black, P. G., F. D. Marks Jr., and R. A. Black, 1986: Supercell structure in tropical cyclones. Preprints, *23d Conf. on Radar Meteorology,* Snowmass, CO, Amer. Meteor. Soc., 255–259.

Black, R. A., 1990: Radar reflectivity–ice water content relationships for use above the melting level in hurricanes. *J. Appl. Meteor.,* **29,** 955–961.

——, and J. Hallett, 1986: Observations of the distribution of ice in hurricanes. *J. Atmos. Sci.,* **43,** 802–822.

——, H. B. Bluestein, and M. L. Black, 1994: Unusually strong vertical motions in a Caribbean hurricane. *Mon. Wea. Rev.,* **122,** 2722–2739.

Bogner, P. B., G. M. Barnes, and J. L. Franklin, 2000: Conditional instability and shear for six hurricanes over the Atlantic Ocean. *Wea. Forecasting,* **15,** 192–207.

Bolton, D., 1980: The computation of equivalent potential temperature. *Mon. Wea. Rev.,* **108,** 1046–1053.

Braun, S. A., 2002: A cloud-resolving simulation of Hurricane Bob (1991): Storm structure and eyewall buoyancy. *Mon. Wea. Rev.,* **130,** 1573–1592.

Cecil, D. J., E. J. Zipser, and S. W. Nesbitt, 2002: Reflectivity, ice scattering, and lightning characteristics of hurricane eyewalls and rainbands. Part I: Quantitative description. *Mon. Wea. Rev.,* **130,** 769–784.

Eastin, M. D., 2003: Buoyancy of convective vertical motions in the inner core of intense hurricanes. Ph.D. dissertation, Colorado State University, 152 pp. [Available from Department of Atmospheric Science, Colorado State University, Fort Collins, CO 80523.]

——, P. G. Black, and W. M. Gray, 2002a: Flight-level instrument wetting errors in hurricanes. Part I: Observations. *Mon. Wea. Rev.,* **130,** 825–841.

——, ——, and ——, 2002b: Flight-level instrument wetting errors in hurricanes. Part II: Implications. *Mon. Wea. Rev.,* **130,** 842–851.

——, W. M. Gray, and P. G. Black, 2005: Buoyancy of convective vertical motions in the inner core of intense hurricanes. Part II: Case studies. *Mon. Wea. Rev.,* **133,** 209–227.

Ebert, E. E., and G. J. Holland, 1992: Observations of record deep convection in Tropical Cyclone Hilda. *Mon. Wea. Rev.,* **120,** 2240–2251.

Emanuel, K. A., 1986: An air–sea interaction theory for tropical cyclones. Part I: Steady-state maintenance. *J. Atmos. Sci.,* **43,** 585–604.

Feind, R. E., A. G. Detweiler, and P. L. Smith, 2000: Cloud liquid water measurements on the Armored T-28: Intercomparisons between Johnson–Williams cloud water meter and CSIRO (king) liquid water probe. *J. Atmos. Oceanic Technol.,* **17,** 1630–1638.

Frank, W. M., 1977: The storm structure and energetics of the tropical cyclone. I. Storm structure. *Mon. Wea. Rev.,* **105,** 1119–1135.

Gamache, J. F., R. A. Houze Jr., and F. D. Marks Jr., 1993: Dual-aircraft investigation of Hurricane Norbert. Part III: Water budget. *J. Atmos. Sci.,* **50,** 3221–3243.

Gentry, R. C., T. T. Fujita, and R. C. Sheets, 1970: Aircraft, spacecraft, satellite, and radar observations of Hurricane Gladys, 1968. *J. Appl. Meteor.,* **9,** 837–850.

Gray, W. M., 1965: Calculations of cumulus draft velocities in hurricanes from aircraft data. *J. Appl. Meteor.,* **4,** 463–474.

——, and D. J. Shea, 1973: The hurricane's inner core region. II. Thermal stability and dynamic characteristics. *J. Atmos. Sci.,* **30,** 1565–1576.

Helfrich, K. R., 1994: Thermals with background rotation and stratification. *J. Fluid Mech.,* **259,** 265–280.

Heymsfield, G. M., J. B. Halverson, J. Simpson, L. Tian, and T. P. Bui, 2001: ER-2 Doppler radar investigations of the eyewall of Hurricane Bonnie during the Convection and Moisture Experiment-3. *J. Appl. Meteor.,* **40,** 1310–1330.

Hock, T. F., and J. L. Franklin, 1999: The NCAR GPS dropwindsonde. *Bull. Amer. Meteor. Soc.,* **80,** 407–420.

Igau, R. C., M. A. LeMone, and D. Wei, 1999: Updraft and downdraft cores in TOGA COARE: Why so many buoyant downdraft cores? *J. Atmos. Sci.,* **56,** 2232–2245.

Jenkins, G. M., and D. G. Watts, 1968: *Spectral Analysis and Its Applications.* Holden-Day, 525 pp.

Jorgensen, D. P., 1984a: Mesoscale and convective-scale characteristics of mature hurricanes. Part I: General observations by aircraft. *J. Atmos. Sci.,* **41,** 1268–1285.

——, 1984b: Mesoscale and convective-scale characteristics of mature hurricanes. Part II: Inner core structure of Hurricane Allen (1980). *J. Atmos. Sci.,* **41,** 1287–1311.

——, and M. A. LeMone, 1989: Vertical velocity characteristics of oceanic convection. *J. Atmos. Sci.,* **46,** 621–640.

——, E. J. Zipser, and M. A. LeMone, 1985: Vertical motions in intense hurricanes. *J. Atmos. Sci.,* **42,** 839–856.

Lawson, R. P., and W. A. Cooper, 1990: Performance of some airborne thermometers in clouds. *J. Atmos. Oceanic Technol.,* **7,** 480–494.

LeMone, M. A., 1980: On the difficulty of measuring temperature and humidity in clouds: Comments on "Shallow convection on day 261 of GATE: Mesoscale arcs." *Mon. Wea. Rev.,* **108,** 1702–1707.

Liu, Y., D.-L. Zhang, and M. K. Yau, 1999: A multiscale numerical study of Hurricane Andrew (1992). Part II: Kinematics and inner-core structures. *Mon. Wea. Rev.,* **127,** 2597–2616.

Lord, S. J., H. E. Willoughby, and J. M. Piotrowicz, 1984: Role of a parameterized ice-phase microphysics in an axisymmetric, nonhydrostatic tropical cyclone model. *J. Atmos. Sci.,* **41,** 2836–2848.

Lucas, C., E. J. Zipser, and M. A. LeMone, 1994: Vertical velocity in oceanic convection off tropical Australia. *J. Atmos. Sci.,* **51,** 3183–3193.

Malkus, J., and H. Riehl, 1960: On the dynamics and energy transformations in steady-state hurricanes. *Tellus,* **12,** 1–20.

——, C. Ronne, and M. Chaffee, 1961: Cloud patterns in Hurricane Daisy, 1958. *Tellus,* **13,** 8–30.

Marks, F. D., Jr., 1985: Evolution of the structure of precipitation in Hurricane Allen (1980). *Mon. Wea. Rev.,* **113,** 909–930.

——, and R. A. Houze Jr., 1987: Inner core structure of Hurricane Alicia from airborne Doppler radar observations. *J. Atmos. Sci.,* **44,** 1296–1317.

——, ——, and J. F. Gamache, 1992: Dual-aircraft investigation of the inner core of Hurricane Norbert (1948). Part I: Kinematic structure. *J. Atmos. Sci.,* **49,** 919–942.

Merceret, F. J., and T. L. Schricker, 1975: A new hot-wire liquid cloud water meter. *J. Appl. Meteor.,* **14,** 319–326.

Montgomery, M. T., and J. L. Franklin, 1998: An assessment of the balance approximation in hurricanes. *J. Atmos. Sci.,* **55,** 2193–2200.

Riehl, H., 1979: *Climate and Weather in the Tropics.* Academic Press, 611 pp.

——, and J. Malkus, 1961: Some aspects of Hurricane Daisy (1958). *Tellus,* **13,** 181–213.

Rotunno, R., and K. A. Emanuel, 1987: An air–sea interaction theory for tropical cyclones. Part II: Evolutionary study using a nonhydrostatic numerical model. *J. Atmos. Sci.,* **44,** 542–561.

Samsury, C. E., and E. J. Zipser, 1995: Secondary wind maxima in hurricanes: Airflow and relationship to rainbands. *Mon. Wea. Rev.,* **123,** 3502–3517.

Shapiro, L. J., and H. E. Willoughby, 1982: The response of balanced hurricanes to local sources of heat and momentum. *J. Atmos. Sci.,* **39,** 378–394.

——, and M. T. Montgomery, 1993: A three-dimensional balance theory for rapidly rotating vortices. *J. Atmos. Sci.,* **50,** 3322–3335.

Shea, D. J., and W. M. Gray, 1973: The hurricane's inner core region. I. Symmetric and asymmetric structure. *J. Atmos. Sci.,* **30,** 1544–1564.

Sheets, R. C., 1969: Some mean hurricane soundings. *J. Appl. Meteor.,* **8,** 134–146.

Spyers-Duran, P. A., 1968: Comparative measurements of cloud liquid water using heated wire and cloud replicating devices. *J. Appl. Meteor.,* **7,** 674–678.

Srivastava, R. C., 1987: A model of intense downdrafts driven by the melting and evaporation of precipitation. *J. Atmos. Sci.,* **44,** 1752–1773.

Wang, J., H. L. Cole, D. J. Carlson, E. R. Miller, K. Beierle, A. Paukkunen, and T. K. Laine, 2002: Corrections of humidity measurement errors from the Vaisala RS80 radiosonde—Application to TOGA COARE data. *J. Atmos. Oceanic Technol.,* **19,** 981–1002.

Wang, Y., 2002: Vortex Rossby waves in a numerically simulated tropical cyclone. Part I: Overall structure, potential vorticity, and kinetic energy budgets. *J. Atmos. Sci.,* **59,** 1213–1238.

Wei, D., A. M. Blyth, and D. J. Raymond, 1998: Buoyancy of convective clouds in TOGA COARE. *J. Atmos. Sci.,* **55,** 3381–3391.

Willoughby, H. E., 1979: Forced secondary circulations in hurricanes. *J. Geophys. Res.,* **84,** 3173–3183.

——, 1990: Gradient balance in tropical cyclones. *J. Atmos. Sci.,* **47,** 265–274.

——, and M. B. Chelmow, 1982: Objective determination of hurricane tracks from aircraft observations. *Mon. Wea. Rev.,* **110,** 1298–1305.

——, J. A. Clos, and M. G. Shoreibah, 1982: Concentric eyewalls, secondary wind maxima, and the evolution of the hurricane vortex. *J. Atmos. Sci.,* **39,** 395–411.

Zhang, D.-L., Y. Liu, and M. K. Yau, 2000: A multiscale numerical study of Hurricane Andrew (1992). Part III: Dynamically induced vertical motion. *Mon. Wea. Rev.,* **128,** 3772–3788.

Zipser, E. J., 2003: Some views on "hot towers" after 50 years of tropical field programs and two years of TRMM data. *Cloud Systems, Hurricanes, and the Tropical Rainfall Measuring Mission (TRMM), Meteor. Monogr.,* No. 51, Amer. Meteor. Soc., 49–58.